

# A Closed-Form Solution for Debiasing Vision-Language Models with Utility Guarantees Across Modalities and Tasks

Tangzheng Lian  
King’s College London  
lian.tangzheng@kcl.ac.uk

Guanyu Hu  
Queen Mary University of London  
g.hu@qmul.ac.uk

Yijing Ren  
King’s College London  
yijing.ren@kcl.ac.uk

Dimitrios Kollias  
Queen Mary University of London  
d.kollias@qmul.ac.uk

Oya Celiktutan  
King’s College London  
oya.celiktutan@kcl.ac.uk

## Abstract

While Vision-Language Models (VLMs) have achieved remarkable performance across diverse downstream tasks, recent studies have shown that they can inherit social biases from the training data and further propagate them into downstream applications. To address this issue, various debiasing approaches have been proposed, yet most of them aim to improve fairness without having a theoretical guarantee that the utility of the model is preserved. In this paper, we introduce a debiasing method that yields a **closed-form** solution in the cross-modal space, achieving Pareto-optimal fairness with **bounded utility losses**. Our method is **training-free**, requires **no annotated data**, and can jointly debias both visual and textual modalities across downstream tasks. Extensive experiments show that our method outperforms existing methods in debiasing VLMs across diverse fairness metrics and datasets for both group and **intersectional** fairness in downstream tasks such as zero-shot image classification, text-to-image retrieval, and text-to-image generation while preserving task performance. Code [https://github.com/Supltz/Debias\\_VLM](https://github.com/Supltz/Debias_VLM).

## 1. Introduction

VLMs such as CLIP (Contrastive Language–Image Pre-training) [36] have been applied and greatly improved performance across a wide range of downstream computer vision tasks by effectively bridging visual and linguistic semantics. This success largely stems from their training on massive collections of web-scraped image–text pairs [39], which enables strong generalization without the need for task-specific supervision. However, as shown in previous literature [3, 9], these web-scraped contents inherently contain harmful stereotypes and spurious correlations arising

from demographic imbalances. For example, in CLIP’s text embeddings, the concept “nurse” is unusually similar to “female”, while “doctor” is unusually similar to “male”, reflecting gender stereotypes that exist in online captions [41]. Similarly, web-scraped images of smiling faces often co-occur more frequently with female-looking faces than male-looking ones, even if there is no causal connection between gender and smiling expression [16, 27]. Such biases or spurious correlations embedded within VLM representations can propagate into downstream applications if left unaddressed [46]. Ensuring algorithmic fairness in VLMs is therefore essential, particularly in human-centered computer vision tasks [28, 49], where discriminatory or stereotypical outputs can severely undermine public trust in AI systems [11, 19, 44].

However, debiasing VLMs has several key challenges:

(1) *Multi-Modal Bias*. Bias in VLMs is encoded in both image and text embeddings by cross-modal alignment. Debiasing only one of them may not be sufficient [51].

(2) *Training Cost*. Retraining VLMs on massive datasets from scratch is computationally impractical. Therefore, many debiasing methods freeze the image and text encoders and train additional debiasing networks on top of the embeddings [2, 7, 41], which not only require extra computational cost but also increase model complexity and inference cost by introducing extra network parameters to the VLMs.

(3) *Sensitive Attribute Annotations*. Debiasing methods in VLMs typically require datasets annotated with sensitive attributes such as gender, race, or age [21, 47]. Collecting such data is challenging due to privacy concerns and ethical constraints [50]. Moreover, perceived attribute annotations are often subjective and require extensive curation [23].

(4) *Diverse Downstream Tasks*. VLMs are applied to a wide range of tasks, each with distinct fairness and utility metrics. Most existing debiasing methods focus on a single task, such as zero-shot image classification [1, 7, 33] or

Table 1. Overview of recent debiasing methods in VLMs.

Methods	SFID [21]	DeAR [41]	CLIP-clip [47]	Fairer CLIP [7]	PRISM [33]	PRISM-mini [33]	SANER [14]	Biased Prompt [5]	Robo Shot [1]	Prompt Array [2]	JointV-L [51]	Ours
Training-Free	✗	✗	✓	✗	✗	✓	✗	✓	✓	✗	✗	✓
Data-Free	✗	✗	✗	✗	✓	✓	✓	✓	✓	✗	✗	✓
Debiasing Both Modalities	✓	✗	✓	✓	✓	✓	✗	✗	✓	✓	✓	✓
Bounded Utility Loss	✗	✗	✗	✗	✗	✗	✗	✗	✗	✗	✗	✓
Zero-Shot Image Classification	✓	✗	✗	✓	✓	✓	✗	✓	✓	✗	✗	✓
Text-to-Image Retrieval	✓	✓	✓	✗	✗	✗	✓	✓	✗	✓	✓	✓
Text-to-Image Generation	✓	✗	✗	✗	✗	✗	✓	✓	✗	✗	✗	✓
Intersectional Fairness	✗	✗	✗	✗	✗	✗	✗	✗	✗	✗	✗	✓

text-to-image retrieval [2, 41, 47, 51], as it remains challenging to design a *unified* debiasing approach with utility preservation across different downstream tasks [17].

(5) *Utility Preservation*. Debiasing VLMs often leads to a reduction in task performance [2, 21, 41]. Preserving downstream utility is challenging due to the inherent utility-fairness trade-off [29]. For example, in text-to-image generation, the input prompt may explicitly request generating male- or female-presenting images. Removing gender information can therefore degrade task performance [14].

Apart from these challenges, we also observe that although intersectional biases have been widely documented in VLMs [12, 15], prior debiasing methods have primarily focused on group fairness [1, 2, 7, 14, 21, 33, 41, 51, 53], which only ensures parity across individual sensitive attributes. However, in real-world scenarios, individuals often belong to multiple sensitive groups simultaneously [24, 34]. The concept of intersectional fairness remains largely underexplored in existing VLM debiasing studies. To bridge these gaps, our contributions are summarized as follows:

(1) We propose a debiasing method that yields a *closed-form* solution in the cross-modal space, achieving Pareto-optimal fairness with provably bounded utility losses.

(2) Our proposed method is *training-free*, requires *no extra data* and *sensitive attribute annotations*, and can debias both visual and textual modalities across multiple tasks.

(3) Extensive experiments show that our method outperforms existing methods in debiasing VLMs across diverse fairness metrics and datasets for both group and *intersectional* fairness in downstream tasks such as zero-shot image classification, text-to-image retrieval, and text-to-image generation, while preserving task performance.

## 2. Related Work

The presence of biases in VLMs has been extensively documented in prior research [12, 15, 18, 38, 45, 48]. In this section, we focus specifically on recent debiasing methods most relevant to our work, as summarized in Table 1.

Many existing methods require both additional training of auxiliary networks and datasets annotated with sensitive attributes. For instance, DeAR [41] introduces a residual

network to maximize the cross-entropy loss for predicting sensitive attributes. PromptArray [2] adopts a similar idea by prepending learnable embeddings and maximizing the prediction error of the adversary. FairerCLIP [7] proposes a dependence metric to minimize the statistical dependence between embeddings and sensitive attributes, and JointV-L [51] proposes to align bias across image and text modalities before applying counterfactual text to train a network.

SFID [21] and CLIP-clip [47] both assume that certain embedding dimensions encode bias. SFID trains a lightweight Random Forest classifier to identify such biased dimensions and replaces them with neutral values, while CLIP-clip offers a training-free alternative by estimating mutual information and clipping those dimensions. However, both methods still require data with sensitive attribute annotations to locate such dimensions. PRISM (training-based) and its variant PRISM-mini (training-free) [33] debias embeddings via projection operations without extra annotations. However, similar to RoboShot [1], they only focus on zero-shot image classification tasks, leaving their applicability for other tasks such as text-to-image retrieval and generation unclear. SANER [14] addresses bias in text-to-image retrieval and generation by proposing attribute neutralization. Although it does not rely on additional annotated data, it is not training-free. BiasedPrompt [5] proposes two training-free methods: Orth-Proj [5] and an extended version, Orth-Cali [5]. However, both methods in Biased-Prompt and SANER focus solely on debiasing textual embeddings while ignoring biases in visual embeddings.

As shown in Table 1, our method is the first to *simultaneously* be training-free, data-free, and can debias both image and text modalities across all three downstream tasks. Regarding utility preservation, some approaches fail to explicitly address this aspect [5], while others, such as DeAR [41] and SANER [14] attempt to preserve it through reconstruction losses. However, the ability to reconstruct embeddings via a trained network does not ensure that the original semantic utility or the cross-modal alignment is retained. Other methods [7, 21, 33] claim utility preservation based on similar objectives and empirical results, often requiring extensive hyperparameter tuning. In contrast, we are the

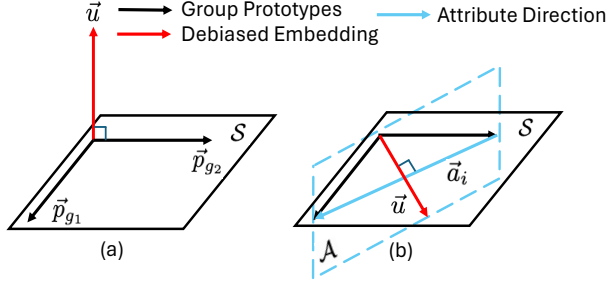


Figure 1. (a) Previous methods such as PRISM-mini [33] and Orth-Proj [5] debias through an orthogonal projection to the subspace  $\mathcal{S}$  spanned by the embeddings of group-explicit prompts (*group prototypes*) such as “a photo of a female/male doctor.” However, the subspace  $\mathcal{S}$  contains not only attribute-related information but also essential semantic content (e.g., “doctor”) that we wish to preserve. (b) We instead debias through an orthogonal projection to the attribute subspace  $\mathcal{A}$  so that  $\vec{u}$  can effectively remove bias while maintaining content-related semantics.

first to provide theoretical bounds on utility losses when debiasing VLMs. Moreover, prior methods primarily focus on group fairness. As noted in [24, 34], they can suffer from *fairness gerrymandering*, where a model that is fair with respect to individual sensitive attributes but still be unfair at their intersections. To address this, we further extend the evaluation to intersectional fairness, capturing more complex and realistic scenarios when debiasing VLMs.

### 3. Problem Formulation

**Notation.** We denote the input image and text of VLMs as  $I_{\text{in}}$  and  $T_{\text{in}}$ , and their corresponding encoders as  $f_I(\cdot)$  and  $f_T(\cdot)$ . The resulting image and text embeddings are  $\vec{e}_I = f_I(I_{\text{in}})$  and  $\vec{e}_T = f_T(T_{\text{in}})$ , respectively. We consider a sensitive attribute  $S$ , such as age, gender, or skin tone, or any intersection of them. Let  $S$  contain  $n \geq 2$  groups and define the set of attribute groups as  $\mathcal{G} = \{g_1, g_2, \dots, g_n\}$ . For example, if  $S$  represents *gender*, then  $\mathcal{G} = \{\text{male, female}\}$ ; if  $S$  represents the intersection of *gender* and *race*, then  $\mathcal{G} = \{(\text{male, light}), (\text{female, dark}), \dots, (\text{female, light})\}$ . We denote  $\vec{u} \in \{\vec{u}_I, \vec{u}_T\}$  as the debaised embedding corresponding to the original embedding  $\vec{e} \in \{\vec{e}_I, \vec{e}_T\}$ , which we aim to find within the cross-modal space<sup>1</sup>  $\mathbb{S}^{d-1}$  for either the image or text modality (see details in Section 4.2).

#### 3.1. Defining the Objectives

**Utility.** We define utility from two perspectives. For downstream tasks that use a single encoder, such as text-to-image generation, we define *Self-Utility* as the preservation of the original semantic content, measured by the cosine similarity between the debaised embedding  $\vec{u}$  and the original em-

<sup>1</sup>The cross-modal space in VLMs is a unit hypersphere  $\mathbb{S}^{d-1}$ , where all embeddings are  $\ell_2$ -normalized and  $d$  is the embedding dimension.

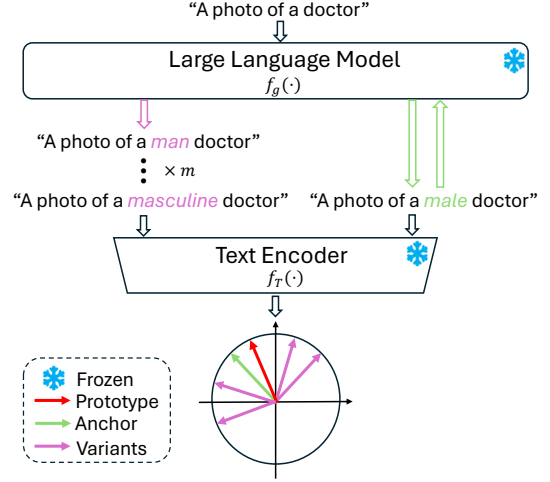


Figure 2. Illustration of the group prototype construction process.

bedding  $\vec{e}$ . We ensure self-utility by minimizing the self-utility loss of which we defined as  $\ell_{self} = 1 - \langle \vec{u}, \vec{e} \rangle$  with a lower value indicating stronger semantic preservation. (2) For downstream tasks that utilize both encoders, such as zero-shot image classification, we define *Cross-Utility* as the preservation of cross-modal alignment between the image–text pair before and after debiasing. We ensure cross-utility by minimizing the cross-utility loss denoted as  $\ell_{cross} = |\langle \vec{u}_I, \vec{u}_T \rangle - \langle \vec{e}_I, \vec{e}_T \rangle|$  with a small value indicating that the image–text alignment is preserved.

**Fairness.** We formulate fairness as neutralization, which requires  $\vec{u}$  to be equally similar<sup>2</sup> to all embeddings of group-explicit prompts (*group prototypes*):  $\langle \vec{u}, \vec{p}_{g_1} \rangle = \langle \vec{u}, \vec{p}_{g_2} \rangle = \dots = \langle \vec{u}, \vec{p}_{g_n} \rangle$ . This condition can be equivalently written as:  $\langle \vec{u}, \vec{a}_i \rangle = 0, \forall i = 2, \dots, n$ , where  $\vec{a}_i = \vec{p}_{g_i} - \vec{p}_{g_1}$  denotes the attribute direction between group prototypes. We thus define the attribute subspace as the span of these directions:  $\mathcal{A} := \text{span}\{\vec{a}_2, \vec{a}_3, \dots, \vec{a}_n\}$ . As shown in Fig 1, compared to [5, 33] that project the embedding orthogonally onto the subspace  $\mathcal{S}$ , which may cause a loss of utility, this formulation ensures that  $\vec{u}$  is orthogonal only to the attribute subspace, preserving the content-related semantics.

### 4. Methodology

Our method consists of two main components. To construct the attribute subspace  $\mathcal{A}$ , for each group  $g$ , the first step builds textual prototypes  $\vec{p}_g$  guided by a large language model (LLM). The second step then searches for the debaised embedding  $\vec{u} \in \mathbb{S}^{d-1}$  while preserving the utilities. Please see **Appendix A** for the proofs of all propositions, lemmas, and theorems introduced in the methodology.

<sup>2</sup>This similarity-based fairness surrogate has been shown to improve multiple fairness metrics across downstream tasks effectively [4, 14].

#### 4.1. LLM-Guided Group Prototype Construction

Given an input prompt<sup>3</sup>  $T_{in}$ , e.g., “a photo of a doctor,” the goal of this module is to construct group prototypes conditioned on  $T_{in}$ . As illustrated in Fig. 2, for each group  $g$ , we first pass  $T_{in}$  to a LLM, denoted as  $f_g(\cdot)$ , which performs two tasks within the same context window: (1) it inserts the group specifications while preserving the rest of the prompt content. For example, with  $g = \text{“male,”}$  we may obtain  $T_g = f_g(T_{in}) = \text{“a photo of a male doctor.”}$  (2) it takes  $T_g$  as input and generates multiple alternative phrasings that express  $g$  while ensuring correct grammar and the rest of the text remains unchanged. For example, this may yield prompts such as “a photo of a man doctor” or “a photo of a masculine doctor.” We denote these variants as  $\mathcal{T}_g = \{T_g^{(1)}, T_g^{(2)}, \dots, T_g^{(m)}\}$ . We use GPT-5 as the LLM while other LLMs are also explored in Section 5.2.1. Please see more details of this module in **Appendix B**.

Previous works [5, 33] directly use  $T_g$  as the group prototype, overlooking that attribute groups are not linguistically monolithic. For instance, terms such as “man,” “gentleman,” and “boy” all convey different connotations of maleness. To address this, SANER [14] constructs a corpus of group-specific words beforehand and inserts them into  $T_{in}$ . However, these words are not conditioned on  $T_{in}$ , which may lead to prompts that are semantically inconsistent with the input text. In contrast, we leverage the reasoning capability of LLMs to construct  $\mathcal{T}_g$ , ensuring better contextual alignment. We denote the embedding for the anchor prompt  $T_g$  as  $\vec{e}_g = f_T(T_g)$ . For the generated variants, we compute  $\mathcal{E}_g = \{\vec{e}_g^{(1)}, \vec{e}_g^{(2)}, \dots, \vec{e}_g^{(m)}\}$ , where the embedding for each variant  $\vec{e}_g^{(i)} = f_T(T_g^{(i)})$ . To construct a representative group prototype, we seek an embedding on  $\mathbb{S}^{d-1}$  that maximizes its cosine similarity with both  $T_g$  and its generated variants, which corresponds to the spherical mean:

$$\vec{p}_g = \frac{\vec{e}_g + \sum_{i=1}^m \vec{e}_g^{(i)}}{\|\vec{e}_g + \sum_{i=1}^m \vec{e}_g^{(i)}\|}.$$

Therefore, for each group  $g$ , we set  $\vec{p}_g$  as the group prototype. These prototypes are then used to construct the attribute space  $\mathcal{A}$ , to which  $\vec{u}$  should be orthogonal.

#### 4.2. Searching the Debaised Embedding $\vec{u} \in \mathbb{S}^{d-1}$

**Preliminaries.** By the orthogonal decomposition theorem [42], any embedding  $\vec{u} \in \mathbb{S}^{d-1}$  can be decomposed as  $\vec{u} = \vec{u}_{\mathcal{A}_{\parallel}} + \vec{u}_{\mathcal{A}_{\perp}}$ , where  $\vec{u}_{\mathcal{A}_{\parallel}} = P_{\mathcal{A}_{\parallel}} \vec{u}$  is the component parallel to  $\mathcal{A}$  (i.e., the attribute leakage), and  $\vec{u}_{\mathcal{A}_{\perp}} = P_{\mathcal{A}_{\perp}} \vec{u}$  is the component orthogonal to  $\mathcal{A}$  (i.e., the neutral content). The projection operators are given by  $P_{\mathcal{A}_{\parallel}} = A(A^T A)^{-1} A^T$

<sup>3</sup>We use the prompt template “a photo of a/an {sth}” only to align with prior debiasing studies [14, 21]. This module is template-agnostic, and the input prompt could also be group-explicit (see **Appendix B**).

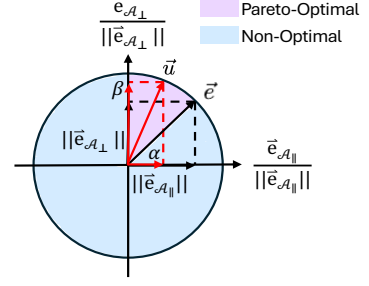


Figure 3. Illustration of the optimal solution space of  $\vec{u}$ .

and  $P_{\mathcal{A}_{\perp}} = I - P_{\mathcal{A}_{\parallel}}$ , where  $I$  is the identity matrix and  $A = [\vec{a}_1, \vec{a}_2, \dots, \vec{a}_r] \in \mathbb{R}^{d \times r}$  is the basis matrix whose columns span  $\mathcal{A}$  with  $r = \text{rank}(A) \leq n - 1 \ll d$ .

**Proposition 1.** The cross-utility loss  $\ell_{cross}$  is upper bounded by  $\sqrt{2} \ell_{self}^{(I)} + \sqrt{2} \ell_{self}^{(T)}$ , where  $\ell_{self}^{(I)}$  and  $\ell_{self}^{(T)}$  are the self-utility loss of image and text embeddings, respectively.

By the decomposition, the fairness objective of finding  $\vec{u}$  to be orthogonal to  $\mathcal{A}$  can be formulated as minimizing attribute leakage ( $\|\vec{u}_{\mathcal{A}_{\parallel}}\| \rightarrow 0$ ). According to **Proposition 1**, the utility objective can be reduced to minimizing only the self-utility loss ( $\ell_{self} \rightarrow 0$ ). Combining both objectives, we formulate a weighted-sum minimization problem as

$$\min_{\vec{u} \in \mathbb{S}^{d-1}} G(\vec{u}) := w_1 \|\vec{u}_{\mathcal{A}_{\parallel}}\| + w_2 (1 - \langle \vec{u}, \vec{e} \rangle), \quad (1)$$

where  $w_1, w_2 \geq 0$  and  $w_1 + w_2 = 1$  denotes the preference.

**Lemma 1.** Every optimal solution  $\vec{u}^*$  of **Problem (1)** satisfies  $\vec{u}^* \in \text{span}\{\vec{e}_{\mathcal{A}_{\parallel}}, \vec{e}_{\mathcal{A}_{\perp}}\}$ , where  $\vec{e}_{\mathcal{A}_{\parallel}}$  and  $\vec{e}_{\mathcal{A}_{\perp}}$  denote the orthogonal components of  $\vec{e}$  with respect to  $\mathcal{A}$ .

Solving **Problem (1)** is challenging because the search space is a unit hypersphere. By **Lemma 1**, the search space can be reduced to the 2D unit circle within  $\text{span}\{\vec{e}_{\mathcal{A}_{\parallel}}, \vec{e}_{\mathcal{A}_{\perp}}\}$ . Hence,  $\vec{u}$  can be represented as  $\vec{u} = \alpha \vec{e}_{\mathcal{A}_{\parallel}} / \|\vec{e}_{\mathcal{A}_{\parallel}}\| + \beta \vec{e}_{\mathcal{A}_{\perp}} / \|\vec{e}_{\mathcal{A}_{\perp}}\|$ , where  $\alpha^2 + \beta^2 = 1$ . By this expression, we can scalarize the vector optimization in **Problem (1)** as

$$\min_{\alpha^2 + \beta^2 = 1} F(\alpha, \beta) := w_1 |\alpha| + w_2 (1 - \alpha \|\vec{e}_{\mathcal{A}_{\parallel}}\| - \beta \|\vec{e}_{\mathcal{A}_{\perp}}\|). \quad (2)$$

**Proposition 2.** Debiasing is unnecessary when **Problem (2)** degenerates into 1D, i.e.,  $\|\vec{e}_{\mathcal{A}_{\parallel}}\| = 0$  or  $\|\vec{e}_{\mathcal{A}_{\perp}}\| = 0$ .

Therefore, we focus on the case where **Problem (2)** remains valid in 2D, i.e.,  $\|\vec{e}_{\mathcal{A}_{\parallel}}\|, \|\vec{e}_{\mathcal{A}_{\perp}}\| \in (0, 1)$ .

**Lemma 2.** The optimal solutions of **Problem (2)** lie in the first quadrant with  $\alpha \in [0, \|\vec{e}_{\mathcal{A}_{\parallel}}\|]$ , which fully characterizes the Pareto front where the attribute leakage and the self-utility loss are strictly increasing and decreasing.

According to **Lemma 2**,  $\vec{u}$  can be expressed solely using  $\alpha$  as  $\vec{u} = \alpha \vec{e}_{\mathcal{A}_{\parallel}} / \|\vec{e}_{\mathcal{A}_{\parallel}}\| + \sqrt{1 - \alpha^2} \vec{e}_{\mathcal{A}_{\perp}} / \|\vec{e}_{\mathcal{A}_{\perp}}\|$  and **Problem (2)** can then be rewritten as

$$\min_{0 \leq \alpha \leq \|\vec{e}_{\mathcal{A}_{\parallel}}\|} F(\alpha) := w_1 L(\alpha) + w_2 V(\alpha), \quad (3)$$

where  $L(\alpha) = \alpha$  is the attribute leakage and  $V(\alpha) = 1 - \alpha \|\vec{e}_{\mathcal{A}_{\parallel}}\| - \sqrt{1 - \alpha^2} \|\vec{e}_{\mathcal{A}_{\perp}}\|$  is the self-utility loss.

As shown in Fig. 3 and **Lemma 2**, we have two extreme cases of **Problem (3)**: (1) **Perfect Utility & Worst Fairness** ( $\alpha = \|\vec{e}_{\mathcal{A}_{\parallel}}\|$ ): in this case,  $\vec{u} = \vec{e}$ , where the self-utility loss attains its minimum,  $V(\alpha) = 1 - \|\vec{e}_{\mathcal{A}_{\parallel}}\|^2 - \|\vec{e}_{\mathcal{A}_{\perp}}\|^2 = 0$  and the attribute leakage reaches its maximum,  $L(\alpha) = \|\vec{e}_{\mathcal{A}_{\parallel}}\|$ . (2) **Perfect Fairness & Worst Utility** ( $\alpha = 0$ ): in this case,  $\vec{u} = \vec{e}_{\mathcal{A}_{\perp}} / \|\vec{e}_{\mathcal{A}_{\perp}}\|$ , where the attribute leakage achieves its minimum,  $L(\alpha) = 0$  and the self-utility loss reaches its maximum,  $V(\alpha) = 1 - \|\vec{e}_{\mathcal{A}_{\perp}}\|$ . This extreme case corresponds exactly to the orthogonal projection operation adopted by previous methods [5, 14, 33].

In contrast, we aim to solve **Problem (3)** to obtain a debiased embedding  $\vec{u}^*$  with  $\alpha^* \in (0, \|\vec{e}_{\mathcal{A}_{\parallel}}\|)$  such that it achieves Pareto-optimal fairness, while the self-utility loss  $\ell_{self}$  is lower than  $1 - \|\vec{e}_{\mathcal{A}_{\perp}}\|$ . According to **Proposition 1**, the cross-utility violation  $\ell_{cross}$  is also upper bounded by  $\sqrt{2(1 - \|\vec{e}_{\mathcal{A}_{\perp}}^{(I)}\|)} + \sqrt{2(1 - \|\vec{e}_{\mathcal{A}_{\perp}}^{(T)}\|)}$ . Since we aim for a *task-agnostic* solution, we do not assume access to any data in the downstream tasks for task-specific tuning and searching ( $w_1, w_2$ ). Thus, we derive the optimal  $\alpha^*$  in **Problem (3)** that remains robust against any admissible  $w_1$  and  $w_2$  by minimizing the worst case via the Chebyshev scalarisation:

$$\min_{0 \leq \alpha \leq \|\vec{e}_{\mathcal{A}_{\parallel}}\|} \sup_{\substack{w_1, w_2 \geq 0 \\ w_1 + w_2 = 1}} \left\{ w_1 L(\alpha) + w_2 V(\alpha) \right\} \quad (4)$$

**Theorem 1.** For any admissible  $w_1$  and  $w_2$ , **Problem (4)** admits a closed-form solution:

$$\alpha^* = \frac{E - \|\vec{e}_{\mathcal{A}_{\perp}}\| \sqrt{E^2 - \|\vec{e}_{\mathcal{A}_{\parallel}}\|^2}}{E^2 + \|\vec{e}_{\mathcal{A}_{\perp}}\|^2}.$$

where  $E := \|\vec{e}_{\mathcal{A}_{\parallel}}\| + (1 - \|\vec{e}_{\mathcal{A}_{\perp}}\|) / \|\vec{e}_{\mathcal{A}_{\parallel}}\|$  and the optimal debiased embedding is  $\vec{u}^* = \sqrt{1 - (\alpha^*)^2} \vec{e}_{\mathcal{A}_{\perp}} / \|\vec{e}_{\mathcal{A}_{\perp}}\| + \alpha^* \vec{e}_{\mathcal{A}_{\parallel}} / \|\vec{e}_{\mathcal{A}_{\parallel}}\|$ . The corresponding attribute leakage and self-utility loss are  $L(\alpha^*) = \alpha^*$  and  $V(\alpha^*) = (1 - \|\vec{e}_{\mathcal{A}_{\perp}}\|) \alpha^* / \|\vec{e}_{\mathcal{A}_{\parallel}}\|$ , while a tighter upper bound on the cross-utility loss is given by

$$\ell_{cross} \leq \sqrt{\frac{2(1 - \|\vec{e}_{\mathcal{A}_{\perp}}^{(I)}\|) \alpha^*}{\|\vec{e}_{\mathcal{A}_{\parallel}}\|}} + \sqrt{\frac{2(1 - \|\vec{e}_{\mathcal{A}_{\perp}}^{(T)}\|) \alpha^*}{\|\vec{e}_{\mathcal{A}_{\parallel}}\|}}.$$

## 5. Downstream Tasks and Their Evaluations

**Zero-Shot Image Classification.** This task jointly uses the image and text encoders to make predictions. Each candidate class is represented by a text prompt “a photo of a/an {class name}” and encoded using the text encoder, while the image encoder encodes the input image. The predicted class is the one whose text embedding has the highest cosine

similarity with the encoded image. Bias in this setting manifests as disparities in performance across sensitive attribute groups for the same class. To quantify this, we adopt the widely used fairness metric *Equal Opportunity (EO)* [13] and measure its violation across groups and classes:

$$\Delta_{EO}^{Avg} = \frac{1}{\mathcal{K}} \sum_{k=1}^{\mathcal{K}} \max_{g, g'} |p_g^k - p_{g'}^k|,$$

$$\Delta_{EO}^{Max} = \max_k \frac{2}{|\mathcal{G}|(|\mathcal{G}| - 1)} \sum_{g, g'} |p_g^k - p_{g'}^k|.$$

Here,  $p_g^k = P(\hat{Y} = k | Y = k, \mathcal{G} = g)$  and  $p_{g'}^k = P(\hat{Y} = k | Y = k, \mathcal{G} = g')$  denote the conditional true positive rates for unordered distinct groups  $g$  and  $g'$ , respectively, while  $\hat{Y}$  and  $Y$  represent the predicted and true class.  $\mathcal{K}$  and  $\mathcal{G}$  denote the number of classes and attribute groups. Since both  $\mathcal{K}$  and  $\mathcal{G}$  can have more than two categories, following prior work [22], we report two variants of EO violation in multi-class or multi-group scenarios: (1)  $\Delta_{EO}^{Avg}$ , which averages the violations across classes and takes the maximum across groups, and (2)  $\Delta_{EO}^{Max}$ , which averages within groups and then takes the maximum across classes. For utility, we use the (macro) F1 score as the evaluation metric.

**Text-to-Image Retrieval.** This task uses the joint matching capability of the image and text encoders in VLMs. Given an input prompt, the model retrieves images from a candidate dataset by ranking them based on the cosine similarity between image and text embeddings. Bias in this task occurs when the proportion of attribute groups in the retrieved results deviates from their original proportions in the candidate dataset. Following prior studies [2, 5, 14, 21, 41], we adopt the *MaxSkew@M* metric to evaluate fairness. Let  $\gamma_g = N_g/N$ , where  $N_g$  denotes the number of images belonging to group  $g$  in the candidate dataset, and  $N$  is the total number of images in the candidate dataset. For each neutral prompt  $t$ , we define  $\hat{\gamma}_g^t = M_g^t/M$ , where  $M_g^t$  is the number of images belonging to group  $g$  in the top- $M$  retrieved images. The *MaxSkew@M* metric is given by:

$$MS@M = \frac{1}{|\mathcal{T}|} \sum_{t \in \mathcal{T}} \max_g \log \left( \frac{\hat{\gamma}_g^t}{\gamma_g} \right),$$

where  $\mathcal{T}$  denotes a set of text queries. For utility evaluation, we follow [2, 21, 47] and use the *Recall@K (R@K)* metric, which measures the probability that the ground-truth image appears among the top- $K$  retrieved results, with  $K = 5, 10$ . Therefore, lower MS@M values indicate better fairness, while higher R@K values reflect stronger retrieval utility.

**Text-to-Image Generation.** Following [5, 14, 21], we consider text-to-image generation as a representative downstream task where only one encoder (text encoder) of a VLM is used. Hence, we debias only the text embeddings

to prevent them from propagating bias into the generative model. Bias in this task occurs when the distribution of attribute groups in generated images is not uniform for a neutral prompt. To quantify this, for each neutral prompt  $t$ , we adopt the *Statistical Parity (SP)* metric [5, 14, 43] to measure the deviation between the group distribution in generated images and the ideal uniform distribution:

$$SP_t = \sqrt{\sum_{g \in \mathcal{G}} \left( \frac{N_g^t}{N^t} - \frac{1}{|\mathcal{G}|} \right)^2},$$

where  $N_g^t$  is the number of generated images belonging to group  $g$  and  $N^t$  is the total number of generated images for each prompt. We use the prompt template “A photo of a/an  $o$ ,” where  $o$  is replaced with an occupation term. The full list of 34 occupations  $\mathcal{T}_o$  is provided in **Appendix C**. For each prompt, we set  $N^t = 100$  with perceived gender (Male or Female) as the sensitive attribute. An unbiased model should yield  $SP_t$  close to zero, while higher values indicate greater bias. To compute  $SP_t$ , attribute annotations of generated images are needed. Following prior works [5, 14], we perform both quantitative and qualitative evaluations for fairness and utility in text-to-image generation.

**Fairness.** For quantitative evaluation, following [21], we use BLIP-2 [26] to automatically annotate perceived gender in generated images. Since BLIP-2 may introduce annotation errors that distort fairness evaluation, qualitative evaluation is also performed. We have three independent annotators to label the top-5 prompts  $\mathcal{T}_o^5 \subset \mathcal{T}_o$  showing the highest  $SP_t$  by BLIP-2. We then report two fairness metrics:  $\overline{SP}_{\mathcal{T}_o}$  that average across  $\mathcal{T}_o$  annotated by BLIP-2 and  $\overline{SP}_5$  that averages across  $\mathcal{T}_o^5$  annotated by humans.

**Utility.** Following [14], we evaluate utility by converting prompts in  $\mathcal{T}_o$  into gender-explicit ones  $\mathcal{T}_e$  (e.g., “a photo of a male doctor”). In this setting, the debiased model should generate images only corresponding to the specified gender. For quantitative evaluation, we use the CLIP score as an automated metric to measure average image–text alignment across  $\mathcal{T}_e$ . For qualitative evaluation, the same three annotators manually identify gender-mismatched images among the top-5 prompts in  $\mathcal{T}_e$  with the lowest CLIP scores. The total number of mismatches is denoted as  $N_I$ , and we report the *generation accuracy* computed as  $\text{Acc}^G = (N_G - N_I)/N_G$ , where  $N_G = 500$  is the total number of generated images. Please refer to more details of the evaluation process in **Appendix D**.

## 5.1. Datasets

We focus on image datasets containing humans, as fairness is more well-defined in such contexts [40]. For zero-shot image classification, we adopt two widely used fairness benchmark datasets: **CelebA** [32] and **FACET** [10]. Following prior works [1, 5, 7, 33], we define a binary classifi-

cation task that predicts hair color (blond vs. non-blond). To explore intersectional fairness, we extend the sensitive attribute to the intersection of perceived gender and age, resulting in four subgroups: Male–Old, Female–Old, Male–Young, and Female–Young. Since CelebA is a face-centric dataset with a binary label space, we additionally employ FACET to explore multi-class classification and full-body human images. The sensitive attribute in FACET is set as perceived gender (Male, Female) only.

For text-to-image retrieval, previous works [5, 14, 41] use datasets such as FairFace [23] and PATA [41] as candidate sets to compute MS@M. However, since these datasets contain only sensitive attribute annotations, they focus solely on fairness evaluation while neglecting task utility. To bridge this gap, we follow [21], which adopts image–caption datasets as the candidate sets. Specifically, we use **Flickr30K** [35] and **COCO2017** [30] to compute both R@K and MS@M (M=1000). The sensitive attribute in Flickr30K is perceived gender (Male, Female), whereas in COCO2017 it is the intersection of perceived gender (Male, Female) and skin tone (Light, Dark). Please refer to **Appendix E** for a detailed description of all datasets used.

## 5.2. Experimental Results

**Zero-Shot Image Classification and Text-to-Image Retrieval.** The VLMs we debias for these two tasks include CLIP [36] with different backbones (ViT-L/14 and ResNet50), as well as other models such as BLIP [25]. Experimental results using CLIP (ViT-L/14) are presented in the main paper, while results for other models are provided in **Appendix F**. We compare our method with the *open-sourced* debiasing approaches in Table 1 that have explicitly examined these tasks: [1, 5, 7, 21, 33] for zero-shot image classification, and [2, 5, 7, 21, 47] for text-to-image retrieval. The experimental results are presented in Tables 8 and 9. Each experiment is conducted by bootstrapping the evaluation datasets, and we report the corresponding means and variances. Despite being both training-free and data-free, our method effectively debiases VLMs on these two tasks across multiple fairness metrics and datasets when compared with existing debiasing methods. Notably, it also maintains high task performance, whereas other methods exhibit notable performance drops.

Based on the empirical observations from our experiments, we further discuss the following key research questions (RQs) when designing debiasing methods for VLMs: **RQ1: Are datasets annotated with sensitive attributes necessary for effective VLM debiasing?**

We find no systematic advantage of ✓ methods over ✗ methods in fairness evaluation across both tasks. In fact, ✓ methods are highly sensitive to the domain of the annotated data. For instance, PromptArray, FairerCLIP, and SFID rely on face-centric datasets such as FairFace

Table 2. Experimental results for zero-shot image classification. (G) denotes perceived gender as the sensitive attribute, and (G×A) denotes the intersection of perceived gender and age as the sensitive attribute.  $\uparrow$  indicates that higher values are better, while  $\downarrow$  indicates that lower values are better. Methods that require or do not require attribute-annotated data are marked with  $\checkmark$  and  $\times$ , respectively. Methods that involve or do not involve training are marked with  $\text{🔥}$  and  $\text{❄️}$ , respectively. Methods that debias only the text encoder are denoted by **T**, while methods that debias both modalities are marked with **I&T**. The results of the debiasing methods with the best means are highlighted in bold with brackets, while the second-best are shown in brackets only. All values reported are scaled by 100 (percentages).

Datasets	CelebA			FACET		
Evaluation Metric	F1 $\uparrow$	$\Delta_{EO}^{Avg}$ (G×A) $\downarrow$	$\Delta_{EO}^{Max}$ (G×A) $\downarrow$	Macro F1 $\uparrow$	$\Delta_{EO}^{Avg}$ (G) $\downarrow$	$\Delta_{EO}^{Max}$ (G) $\downarrow$
Baseline CLIP (ViT-L/14)	54.0±0.5	25.1±0.3	45.0±0.3	70.8±0.2	8.9±0.2	49.8±0.3
$\checkmark$ $\text{🔥}$ <b>I&amp;T</b> SFID [21]	52.8±0.5	23.9±0.1	41.6±0.2	69.2±0.3	9.3±0.4	49.8±0.2
$\checkmark$ $\text{🔥}$ <b>I&amp;T</b> FairerCLIP [7]	[53.1]±0.2	24.0±0.1	41.4±0.3	[69.8]±0.2	9.2±0.2	50.1±0.4
$\times$ $\text{🔥}$ <b>I&amp;T</b> PRISM [33]	52.9±0.4	23.9±0.5	40.6±0.1	69.0±0.2	<b>[8.1]</b> ±0.3	48.3±0.3
$\times$ $\text{❄️}$ <b>I&amp;T</b> PRISM-mini [33]	50.4±0.1	24.2±0.6	40.8±0.3	69.2±0.4	8.6±0.2	49.2±0.5
$\times$ $\text{❄️}$ <b>I&amp;T</b> RoboShot [1]	52.3±0.4	<b>[23.3]</b> ±0.2	<b>[40.0]</b> ±0.3	69.3±0.3	8.5±0.1	<b>[47.3]</b> ±0.5
$\times$ $\text{❄️}$ <b>T</b> Orth-Proj [5]	49.3±0.6	26.0±0.2	42.1±0.4	68.6±0.3	9.0±0.5	50.2±0.1
$\times$ $\text{❄️}$ <b>T</b> Orth-Cali [5]	50.1±0.2	26.1±0.4	42.4±0.6	69.3±0.1	9.2±0.3	50.4±0.5
$\times$ $\text{❄️}$ <b>I&amp;T</b> Ours	<b>[56.5]</b> ±0.5	[23.6]±0.3	[40.1]±0.3	<b>[70.7]</b> ±0.4	[8.3]±0.1	[47.5]±0.4

Table 3. Experimental results for text-to-image retrieval. The markers follow the same notation style as in Table 8. (G×ST) denotes the intersection of perceived gender and skin tone. All values reported are scaled by 100 (percentages).

Datasets	COCO2017			Flickr30K		
Evaluation Metric	R@5 $\uparrow$	R@10 $\uparrow$	MS@1000 (G×ST) $\downarrow$	R@5 $\uparrow$	R@10 $\uparrow$	MS@1000 (G) $\downarrow$
Baseline CLIP (ViT-L/14)	83.8±0.3	90.1±0.4	13.4±0.5	91.0±0.6	95.4±0.4	20.3±0.3
$\checkmark$ $\text{🔥}$ <b>I&amp;T</b> SFID [21]	[77.4]±0.4	86.6±0.2	13.2±0.3	86.8±0.3	90.7±0.5	13.6±0.5
$\checkmark$ $\text{🔥}$ <b>I&amp;T</b> PromptArray [2]	77.2±0.6	[86.7]±0.5	12.8±0.4	87.2±0.2	92.4±0.1	12.9±0.4
$\checkmark$ $\text{🔥}$ <b>I&amp;T</b> FairerCLIP [7]	76.8±0.3	85.4±0.4	10.2±0.6	[87.9]±0.5	[92.5]±0.6	12.2±0.5
$\checkmark$ $\text{❄️}$ <b>I&amp;T</b> CLIP-clip [47]	76.1±0.2	85.2±0.3	<b>[9.9]</b> ±0.4	87.7±0.3	91.5±0.1	<b>[11.7]</b> ±0.5
$\times$ $\text{❄️}$ <b>T</b> Orth-Proj [5]	74.5±0.4	83.6±0.3	13.6±0.5	84.4±0.2	88.9±0.1	14.1±0.2
$\times$ $\text{❄️}$ <b>T</b> Orth-Cali [5]	75.2±0.5	84.9±0.4	13.8±0.2	85.3±0.4	90.7±0.3	14.3±0.6
$\times$ $\text{❄️}$ <b>I&amp;T</b> Ours	<b>[81.1]</b> ±0.3	<b>[89.0]</b> ±0.5	[10.1]±0.4	<b>[90.4]</b> ±0.5	<b>[94.9]</b> ±0.2	[11.8]±0.3

to train their debiasing networks, resulting in poor performance on full-body datasets with diverse scenes like FACET, COCO2017, and Flickr30K. As noted in [41, 51], to achieve robust debiasing,  $\checkmark$  methods require diverse annotated datasets covering multiple domains of images. However, collecting such large and diverse datasets with sensitive attribute labels is challenging in practice. In contrast,  $\times$  methods overcome this limitation by exploring the generalizable representations encoded in CLIP, enabling effective debiasing without explicit attribute annotations.

### RQ2: Is training an additional mapping network necessary for effective VLM debiasing?

We find no systematic advantage of  $\text{🔥}$  methods over  $\text{❄️}$  methods in fairness evaluation across both tasks. As illustrated in Fig. 3, we have proved that the region of Pareto-optimal debiased embeddings in the cross-modal space can be characterized through the orthogonal decomposition of the input embedding. Therefore, we argue that training an additional mapping network may complicate the problem.

### RQ3: Is it necessary to debias both image and text?

For methods that are both  $\times$  and  $\text{❄️}$ , we observe that

**I&T** methods consistently outperform **T** methods on fairness metrics across both tasks. As noted in [51], this is because zero-shot image classification and text-to-image retrieval rely on both image and text embeddings, where biases are jointly encoded when aligning them through contrastive learning. This point is also confirmed by the ablation study of our method in Section 5.2.1.

**Text-to-Image Generation.** We debias the Stable Diffusion (SD) v2.1 model [37] using its default implementation. We compare our method with the *open-sourced* debiasing methods [5, 21] in Table 1, which have explicitly examined this task. As shown in Fig. 12, our method generates balanced gender distributions for neutral prompts while effectively preserving model utility for gender-explicit ones with fewer wrong generations. The quantitative and qualitative results in Table 4 further demonstrate that our method achieves competitive debiasing performance while being the best in preserving utility compared with existing methods. Although Orth-Proj and Orth-Cali can effectively reduce bias, they do not explicitly address utility preservation, leading to lower CLIP scores and  $\text{Acc}^G$ .



Figure 4. Illustrative examples for  $o = \text{“doctor”}$ . We randomly sample ten generated images for each method. Female-looking samples are marked in red and numbered. On the left, a more balanced ratio of female- and male-looking samples indicates lower bias, while on the right, fewer female-looking samples reflect better preservation of self-utility (see **Appendix G** for more examples with other occupations).

Table 4. Experimental results for text-to-image generation. All values reported are scaled by 100 (percentages).

Methods	$\overline{SP}_{\mathcal{T}_o} \downarrow$	$\overline{SP}_5 \downarrow$	$\text{CLIP}_{\text{score}} (\%) \uparrow$	$\text{Acc}^G (\%) \uparrow$
Baseline SD v2.1	47.9	58.6	32.8	75.4
Orth-Proj [5]	[39.6]	[28.4]	19.7	53.4
Orth-Cali [5]	41.5	29.2	20.7	56.6
SFID [21]	41.1	29.4	[22.6]	[67.2]
Ours	[39.7]	[28.8]	[24.2]	[74.6]

Table 5. Experimental results of ablation studies and sensitivity analyses on different LLMs.  $\vec{p}_a$  denotes the anchor embedding while  $\vec{p}_m$  denotes the mean embedding across its variants.

Datasets	Flickr30K	CelebA
Metrics	$\text{MS@1000 (G)} \downarrow$	$\Delta_{\text{EO}}^{\text{Max}} (\text{G} \times \text{A}) \downarrow$
Baseline CLIP (ViT-L/14)	$20.3 \pm 0.3$	$45.0 \pm 0.3$
debias with only $\vec{p}_a$	$13.4 \pm 0.5$	$41.1 \pm 0.4$
debias with only $\vec{p}_m$	$14.1 \pm 0.4$	$41.8 \pm 0.5$
debias with DeepSeek v3.2 [31]	$[12.0] \pm 0.3$	$[40.1] \pm 0.4$
debias with Gemini2.5 Pro [6]	$[11.8] \pm 0.6$	$[40.4] \pm 0.2$
debias with only $\vec{u}_I$	$13.4 \pm 0.4$	$41.7 \pm 0.5$
debias with only $\vec{u}_T$	$13.3 \pm 0.6$	$41.1 \pm 0.3$
Ours	$[11.8] \pm 0.3$	$[40.1] \pm 0.3$

### 5.2.1. Ablation Study & Sensitivity Analyses

We conduct ablation studies to evaluate the debiasing performance of our method and its sensitivity to different LLMs using the Flickr30K and CelebA as example datasets. As shown in Table 5, using only the anchor embedding  $\vec{p}_a$  or only the mean embedding  $\vec{p}_m$  as the prototype results in poorer fairness metrics, validating the effectiveness of our proposed group prototype construction module. Moreover, applying debiasing to only one modality also leads to degraded debiasing performance on both datasets, con-

firmed the necessity of jointly debiasing both modalities. Finally, our sensitivity analysis shows that different LLMs have minimal impact on debiasing performance. We attribute this to the simplicity of our prototype generation process, which can be easily handled by modern LLMs.

## 6. Conclusion

In this paper, we propose a *unified* method that can debias VLMs while maintaining their utility across multiple downstream tasks. To this end, we derive a closed-form solution in the cross-modal space that attains Pareto-optimal fairness with bounded utility losses. Our method is *simple yet effective*, can be easily plugged into any VLM, and it enjoys good properties such as being training-free, data-free, and capable of debiasing both image and text modalities. Extensive experiments show that our approach consistently outperforms existing VLM debiasing methods across multiple fairness metrics and datasets for both group and *inter-sectional* fairness while effectively preserving utility.

**Limitations.** Our method focuses on debiasing within the cross-modal space constructed by the image and text encoders of VLMs. Thus, the utility guarantee is defined in this geometric space: it ensures semantic consistency within the VLM representation rather than directly guaranteeing performance on task-specific utility metrics such as F1 score or Recall@K. Extending the debiasing framework to image or text decoders for generative tasks is left for future work. In addition, due to limitations in existing fairness datasets, the attribute groups considered may not fully capture the full spectrum of sensitive attributes. Nonetheless, this does not undermine our methodological contribution, as our framework can accommodate any number of groups.

**Ethical Statement.** The sensitive attributes used in this work are either perceived or linguistically defined and do not correspond to the self-identification of any individual.

## Acknowledgments

Tangzheng Lian is fully funded by the PhD studentship in the Faculty of Natural, Mathematical and Engineering Sciences (NMES) at King’s College London.

## References

- [1] Dyah Adila, Changho Shin, Linrong Cai, and Frederic Sala. Zero-shot robustification of zero-shot models with auxiliary foundation models. In *The Thirteenth International Conference on Learning Representations*, 2023. 1, 2, 6, 7
- [2] Hugo Berg, Siobhan Hall, Yash Bhalgat, Hannah Kirk, Aleksandar Shtedritski, and Max Bain. A prompt array keeps the bias away: Debiasing vision-language models with adversarial learning. In *Proceedings of the 2nd Conference of the Asia-Pacific Chapter of the Association for Computational Linguistics and the 12th International Joint Conference on Natural Language Processing (Volume 1: Long Papers)*, pages 806–822, Online only, 2022. Association for Computational Linguistics. 1, 2, 5, 6, 7
- [3] Abeba Birhane, Sepehr Dehdashtian, Vinay Prabhu, and Vishnu Boddeti. The dark side of dataset scaling: Evaluating racial classification in multimodal models. In *Proceedings of the 2024 ACM Conference on Fairness, Accountability, and Transparency*, pages 1229–1244, 2024. 1
- [4] Tolga Bolukbasi, Kai-Wei Chang, James Y Zou, Venkatesh Saligrama, and Adam T Kalai. Man is to computer programmer as woman is to homemaker? debiasing word embeddings. *Advances in neural information processing systems*, 29, 2016. 3
- [5] Ching-Yao Chuang, Varun Jampani, Yuanzhen Li, Antonio Torralba, and Stefanie Jegelka. Debiasing vision-language models via biased prompts. *arXiv preprint arXiv:2302.00070*, 2023. 2, 3, 4, 5, 6, 7, 8, 9
- [6] Gheorghie Comanici, Eric Bieber, Mike Schaekermann, Ice Pasupat, Noveen Sachdeva, Inderjit Dhillon, Marcel Blisstein, Ori Ram, Dan Zhang, Evan Rosen, et al. Gemini 2.5: Pushing the frontier with advanced reasoning, multimodality, long context, and next generation agentic capabilities. *arXiv preprint arXiv:2507.06261*, 2025. 8
- [7] Sepehr Dehdashtian, Lan Wang, and Vishnu Naresh Boddeti. Fairerclip: Debiasing clip’s zero-shot predictions using functions in rkhs. In *International Conference on Learning Representations (ICLR)*, 2024. 1, 2, 6, 7
- [8] Felix Friedrich, Manuel Brack, Lukas Struppek, Dominik Hintersdorf, Patrick Schramowski, Sasha Luccioni, and Kristian Kersting. Fair diffusion: Instructing text-to-image generation models on fairness. *arXiv preprint arXiv:2302.10893*, 2023. 8
- [9] Noa Garcia, Yusuke Hirota, Yankun Wu, and Yuta Nakashima. Uncurated image-text datasets: Shedding light on demographic bias. In *Proceedings of the IEEE/CVF Conference on Computer Vision and Pattern Recognition*, pages 6957–6966, 2023. 1
- [10] Laura Gustafson, Chloe Rolland, Nikhila Ravi, Quentin Duval, Aaron Adcock, Cheng-Yang Fu, Melissa Hall, and Candace Ross. Facet: Fairness in computer vision evaluation benchmark. In *Proceedings of the IEEE/CVF international conference on computer vision*, pages 20370–20382, 2023. 6
- [11] Thilo Hagendorff. The ethics of ai ethics: An evaluation of guidelines. *Minds and machines*, 30(1):99–120, 2020. 1
- [12] Kimia Hamidieh, Haoran Zhang, Walter Gerych, Thomas Hartvigsen, and Marzyeh Ghassemi. Identifying implicit social biases in vision-language models. In *Proceedings of the AAAI/ACM Conference on AI, Ethics, and Society*, pages 547–561, 2024. 2
- [13] Moritz Hardt, Eric Price, and Nati Srebro. Equality of opportunity in supervised learning. *Advances in neural information processing systems*, 29, 2016. 5
- [14] Yusuke Hirota, Min-Hung Chen, Chien-Yi Wang, Yuta Nakashima, Yu-Chiang Frank Wang, and Ryo Hachiuma. SANER: Annotation-free societal attribute neutralizer for debiasing CLIP. In *The Thirteenth International Conference on Learning Representations*, 2025. 2, 3, 4, 5, 6, 8
- [15] Phillip Howard, Avinash Madasu, Tiep Le, Gustavo Lujan Moreno, Anahita Bhiwandiwalla, and Vasudev Lal. Social-counterfactuals: Probing and mitigating intersectional social biases in vision-language models with counterfactual examples. In *Proceedings of the IEEE/CVF Conference on Computer Vision and Pattern Recognition (CVPR)*, pages 11975–11985, 2024. 2
- [16] Guanyu Hu, Tangzheng Lian, Dimitrios Kollias, Oya Celiktutan, and Xinyu Yang. Causal affect: Causal discovery for facial affective understanding. *arXiv preprint arXiv:2512.00456*, 2025. 1
- [17] Guanyu Hu, Tangzheng Lian, Na Yan, Dimitrios Kollias, Xinyu Yang, Oya Celiktutan, Siyang Song, and Zeyu Fu. Fairmt: Fairness for heterogeneous multi-task learning. *arXiv preprint arXiv:2512.00469*, 2025. 2
- [18] Yukun Jiang, Zheng Li, Xinyue Shen, Yugeng Liu, Michael Backes, and Yang Zhang. ModSCAN: Measuring stereotypical bias in large vision-language models from vision and language modalities. In *Proceedings of the 2024 Conference on Empirical Methods in Natural Language Processing*, pages 12814–12845, Miami, Florida, USA, 2024. Association for Computational Linguistics. 2
- [19] Anna Jobin, Marcello Ienca, and Effy Vayena. The global landscape of ai ethics guidelines. *Nature machine intelligence*, 1(9):389–399, 2019. 1
- [20] Glenn Jocher, Ayush Chaurasia, Alex Stoken, Jirka Borovec, NanoCode012, Yonghye Kwon, Kalen Michael, TaoXie, Ji-acong Fang, imyhxy, Lorna, Yifu Zeng, Colin Wong, Abhiram V, Diego Montes, Zhiqiang Wang, Cristi Fati, Jebastin Nadar, Laughing, and Mrinal Jain. ultralytics/yolov5: v7.0 - yolov5 sota realtime instance segmentation (v7.0), 2022. 9
- [21] Hoin Jung, Taeuk Jang, and Xiaoqian Wang. A unified debiasing approach for vision-language models across modalities and tasks. *Advances in Neural Information Processing Systems*, 37:21034–21058, 2024. 1, 2, 4, 5, 6, 7, 8, 9
- [22] Sangwon Jung, Sanghyuk Chun, and Taesup Moon. Learning fair classifiers with partially annotated group labels. In *Proceedings of the IEEE/CVF conference on computer vision and pattern recognition*, pages 10348–10357, 2022. 5
- [23] Kimmo Karkkainen and Jungseock Joo. Fairface: Face attribute dataset for balanced race, gender, and age for

- bias measurement and mitigation. In *Proceedings of the IEEE/CVF winter conference on applications of computer vision*, pages 1548–1558, 2021. 1, 6
- [24] Michael Kearns, Seth Neel, Aaron Roth, and Zhiwei Steven Wu. Preventing fairness gerrymandering: Auditing and learning for subgroup fairness. In *International conference on machine learning*, pages 2564–2572. PMLR, 2018. 2, 3
- [25] Junnan Li, Dongxu Li, Caiming Xiong, and Steven Hoi. Blip: Bootstrapping language-image pre-training for unified vision-language understanding and generation. In *International conference on machine learning*, pages 12888–12900. PMLR, 2022. 6
- [26] Junnan Li, Dongxu Li, Silvio Savarese, and Steven Hoi. Blip-2: Bootstrapping language-image pre-training with frozen image encoders and large language models. In *International conference on machine learning*, pages 19730–19742. PMLR, 2023. 6
- [27] Tangzheng Lian and Oya Celiktutan. A feature-level framework for evaluating demographic biases in facial expression recognition models. *IEEE Transactions on Affective Computing*, 2026. 1
- [28] Tangzheng Lian, David Adama, Pedro Machado, and Doratha Vinkemeier. Supervised contrastive learning with identity-label embeddings for facial action unit recognition. In *34th British Machine Vision Conference*. British Machine Vision Association, 2023. 1
- [29] Tangzheng Lian, Guanyu Hu, Dimitrios Kollias, Xinyu Yang, and Oya Celiktutan. Fair domain generalization: An information-theoretic view. *arXiv preprint arXiv:2507.05823*, 2025. 2
- [30] Tsung-Yi Lin, Michael Maire, Serge Belongie, James Hays, Pietro Perona, Deva Ramanan, Piotr Dollár, and C Lawrence Zitnick. Microsoft coco: Common objects in context. In *European conference on computer vision*, pages 740–755. Springer, 2014. 6
- [31] Aixin Liu, Bei Feng, Bing Xue, Bingxuan Wang, Bochao Wu, Chengda Lu, Chenggang Zhao, Chengqi Deng, Chenyu Zhang, Chong Ruan, et al. Deepseek-v3 technical report. *arXiv preprint arXiv:2412.19437*, 2024. 8
- [32] Zifei Liu, Ping Luo, Xiaogang Wang, and Xiaoou Tang. Deep learning face attributes in the wild. In *Proceedings of International Conference on Computer Vision (ICCV)*, 2015. 6
- [33] Mahdiyar Molahasani, Azadeh Motamedi, Michael Greenspan, Il-Min Kim, and Ali Etemad. Prism: Reducing spurious implicit biases in vision-language models with llm-guided embedding projection. In *Proceedings of the IEEE/CVF International Conference on Computer Vision*, pages 688–697, 2025. 1, 2, 3, 4, 5, 6, 7
- [34] Mathieu Molina and Patrick Loiseau. Bounding and approximating intersectional fairness through marginal fairness. *Advances in Neural Information Processing Systems*, 35:16796–16807, 2022. 2, 3
- [35] Bryan A Plummer, Liwei Wang, Chris M Cervantes, Juan C Caicedo, Julia Hockenmaier, and Svetlana Lazebnik. Flickr30k entities: Collecting region-to-phrase correspondences for richer image-to-sentence models. In *Proceedings of the IEEE international conference on computer vision*, pages 2641–2649, 2015. 6
- [36] Alec Radford, Jong Wook Kim, Chris Hallacy, Aditya Ramesh, Gabriel Goh, Sandhini Agarwal, Girish Sastry, Amanda Askell, Pamela Mishkin, Jack Clark, et al. Learning transferable visual models from natural language supervision. In *International conference on machine learning*, pages 8748–8763. PMLR, 2021. 1, 6
- [37] Robin Rombach, Andreas Blattmann, Dominik Lorenz, Patrick Esser, and Björn Ommer. High-resolution image synthesis with latent diffusion models. In *Proceedings of the IEEE/CVF conference on computer vision and pattern recognition*, pages 10684–10695, 2022. 7
- [38] Gabriele Ruggeri, Debora Nozza, et al. A multi-dimensional study on bias in vision-language models. In *Findings of the Association for Computational Linguistics: ACL 2023*. Association for Computational Linguistics, 2023. 2
- [39] Christoph Schuhmann, Richard Vencu, Romain Beaumont, Robert Kaczmarczyk, Clayton Mullis, Aarush Katta, Theo Coombes, Jenia Jitsev, and Aran Komatsuzaki. Laion-400m: Open dataset of clip-filtered 400 million image-text pairs. *arXiv preprint arXiv:2111.02114*, 2021. 1
- [40] Andrew D. Selbst, Danah Boyd, Sorelle A. Friedler, Suresh Venkatasubramanian, and Janet Vertesi. Fairness and abstraction in sociotechnical systems. In *Proceedings of the Conference on Fairness, Accountability, and Transparency*, page 59–68, New York, NY, USA, 2019. Association for Computing Machinery. 6
- [41] Ashish Seth, Mayur Hemani, and Chirag Agarwal. Dear: Debiasing vision-language models with additive residuals. In *Proceedings of the IEEE/CVF Conference on Computer Vision and Pattern Recognition*, pages 6820–6829, 2023. 1, 2, 5, 6, 7
- [42] Gilbert Strang. The fundamental theorem of linear algebra. *The American Mathematical Monthly*, 100(9):848–855, 1993. 4
- [43] Christopher Teo, Milad Abdollahzadeh, and Ngai-Man Man Cheung. On measuring fairness in generative models. *Advances in Neural Information Processing Systems*, 36:10644–10656, 2023. 6
- [44] Scott Thiebes, Sebastian Lins, and Ali Sunyaev. Trustworthy artificial intelligence. *Electronic Markets*, 31(2):447–464, 2021. 1
- [45] An Vo, Khai-Nguyen Nguyen, Mohammad Reza Tarsi, Vy Tuong Dang, Anh Totti Nguyen, and Daeyoung Kim. Vision language models are biased. *arXiv preprint arXiv:2505.23941*, 2025. 2
- [46] Angelina Wang and Olga Russakovsky. Overwriting pre-trained bias with finetuning data. In *Proceedings of the IEEE/CVF international conference on computer vision*, pages 3957–3968, 2023. 1
- [47] Jialu Wang, Yang Liu, and Xin Wang. Are gender-neutral queries really gender-neutral? mitigating gender bias in image search. In *Proceedings of the 2021 Conference on Empirical Methods in Natural Language Processing*, pages 1995–2008, Online and Punta Cana, Dominican Republic, 2021. Association for Computational Linguistics. 1, 2, 5, 6, 7

- [48] Zhaotian Weng, Zijun Gao, Jerone Andrews, and Jieyu Zhao. Images speak louder than words: Understanding and mitigating bias in vision-language model from a causal mediation perspective. In *Proceedings of the 2024 Conference on Empirical Methods in Natural Language Processing*, pages 15669–15680, 2024. [2](#)
- [49] Wenqi Xu, Tangzheng Lian, Wei Liu, and Kaili Zhao. Attention-guided soft ranking loss for resource-constrained head pose estimation. In *2021 7th IEEE International Conference on Network Intelligence and Digital Content (IC-NIDC)*, pages 148–152. IEEE, 2021. [1](#)
- [50] Kaiyu Yang, Klint Qinami, Li Fei-Fei, Jia Deng, and Olga Russakovsky. Towards fairer datasets: Filtering and balancing the distribution of the people subtree in the imagenet hierarchy. In *Proceedings of the 2020 conference on fairness, accountability, and transparency*, pages 547–558, 2020. [1](#)
- [51] Haoyu Zhang, Yangyang Guo, and Mohan Kankanhalli. Joint vision-language social bias removal for clip. In *Proceedings of the Computer Vision and Pattern Recognition Conference*, pages 4246–4255, 2025. [1](#), [2](#), [7](#)
- [52] Dora Zhao, Angelina Wang, and Olga Russakovsky. Understanding and evaluating racial biases in image captioning. In *Proceedings of the IEEE/CVF international conference on computer vision*, pages 14830–14840, 2021. [9](#)
- [53] Dachuan Zhao, Weiyue Li, Zhenda Shen, Yushu Qiu, Bowen Xu, Haoyu Chen, and Yongchao Chen. Bias is a subspace, not a coordinate: A geometric rethinking of post-hoc debiasing in vision-language models. *arXiv preprint arXiv:2511.18123*, 2025. [2](#)

# A Closed-Form Solution for Debiasing Vision-Language Models with Utility Guarantees Across Modalities and Tasks

## Supplementary Material

### Overview

1. **Appendix A:** Proofs of the propositions, lemmas, and theorems.
2. **Appendix B:** Details of the LLM-guided group prototype construction module.
3. **Appendix C:** The occupation list and its group-explicit variants used in text-to-image generation.
4. **Appendix D:** The evaluation process in text-to-image generation.
5. **Appendix E:** Detailed descriptions of the datasets used.
6. **Appendix F:** Experimental results for CLIP (ResNet50) and BLIP.
7. **Appendix G:** More illustrative examples for text-to-image generation.

### A. Proofs

**Proof of Proposition 1.** Denote the self-utility losses for the image and text as  $\ell_{\text{self}}^{(I)} := 1 - \langle \vec{u}_I, \vec{e}_I \rangle$  and  $\ell_{\text{self}}^{(T)} := 1 - \langle \vec{u}_T, \vec{e}_T \rangle$ . For the cross-utility loss, we have

$$\begin{aligned}
 \ell_{\text{cross}} &= |\langle \vec{u}_I, \vec{u}_T \rangle - \langle \vec{e}_I, \vec{e}_T \rangle| = |\langle \vec{u}_I, \vec{u}_T \rangle - \langle \vec{e}_I, \vec{u}_T \rangle + \langle \vec{e}_I, \vec{u}_T \rangle - \langle \vec{e}_I, \vec{e}_T \rangle| \\
 &\stackrel{(1)}{\leq} |\langle \vec{u}_I, \vec{u}_T \rangle - \langle \vec{e}_I, \vec{u}_T \rangle| + |\langle \vec{e}_I, \vec{u}_T \rangle - \langle \vec{e}_I, \vec{e}_T \rangle| \\
 &= |\langle \vec{u}_I - \vec{e}_I, \vec{u}_T \rangle| + |\langle \vec{e}_I, \vec{u}_T - \vec{e}_T \rangle| \\
 &\stackrel{(2)}{\leq} \|\vec{u}_I - \vec{e}_I\| \|\vec{u}_T\| + \|\vec{e}_I\| \|\vec{u}_T - \vec{e}_T\| \\
 &= \|\vec{u}_I - \vec{e}_I\| + \|\vec{u}_T - \vec{e}_T\|.
 \end{aligned}$$

Here,  $\stackrel{(1)}{\leq}$  and  $\stackrel{(2)}{\leq}$  are because of the triangle inequality and Cauchy–Schwarz inequalities. For any unit vectors  $\vec{u}, \vec{e}$ , we have

$$\|\vec{u} - \vec{e}\|^2 = \|\vec{u}\|^2 + \|\vec{e}\|^2 - 2\langle \vec{u}, \vec{e} \rangle = 2(1 - \langle \vec{u}, \vec{e} \rangle) = 2\ell_{\text{self}},$$

Applying this to image and text gives

$$\|\vec{u}_I - \vec{e}_I\| = \sqrt{2\ell_{\text{self}}^{(I)}}, \quad \|\vec{u}_T - \vec{e}_T\| = \sqrt{2\ell_{\text{self}}^{(T)}}.$$

Then

$$\ell_{\text{cross}} \leq \|\vec{u}_I - \vec{e}_I\| + \|\vec{u}_T - \vec{e}_T\| = \sqrt{2\ell_{\text{self}}^{(I)}} + \sqrt{2\ell_{\text{self}}^{(T)}}$$

□

**Proof of Lemma 1.** The objective function in **Problem (1)** can be rewritten as

$$\begin{aligned}
 G(\vec{u}) &= w_1 \|\vec{u}_{\mathcal{A}_{\parallel}}\| + w_2 (1 - \langle \vec{u}, \vec{e} \rangle) \\
 &= w_1 \|\vec{u}_{\mathcal{A}_{\parallel}}\| + w_2 \left[ 1 - (\langle \vec{u}_{\mathcal{A}_{\parallel}}, \vec{e}_{\mathcal{A}_{\parallel}} \rangle + \langle \vec{u}_{\mathcal{A}_{\perp}}, \vec{e}_{\mathcal{A}_{\perp}} \rangle) \right] \\
 &\stackrel{(1)}{\geq} w_1 \|\vec{u}_{\mathcal{A}_{\parallel}}\| + w_2 \left[ 1 - (\|\vec{u}_{\mathcal{A}_{\parallel}}\| \|\vec{e}_{\mathcal{A}_{\parallel}}\| + \|\vec{u}_{\mathcal{A}_{\perp}}\| \|\vec{e}_{\mathcal{A}_{\perp}}\|) \right]
 \end{aligned}$$

Here,  $\stackrel{(1)}{\geq}$  is because the Cauchy-Schwarz inequality  $\langle \vec{u}_{\mathcal{A}_{\parallel}}, \vec{e}_{\mathcal{A}_{\parallel}} \rangle + \langle \vec{u}_{\mathcal{A}_{\perp}}, \vec{e}_{\mathcal{A}_{\perp}} \rangle \leq \|\vec{u}_{\mathcal{A}_{\parallel}}\| \|\vec{e}_{\mathcal{A}_{\parallel}}\| + \|\vec{u}_{\mathcal{A}_{\perp}}\| \|\vec{e}_{\mathcal{A}_{\perp}}\|$  with the equality holds *iff* both components of the orthogonal decompositions of  $\vec{u}$  and  $\vec{e}$  are collinear, i.e.,  $\vec{u}_{\mathcal{A}_{\parallel}} \parallel \vec{e}_{\mathcal{A}_{\parallel}}$  and

$\vec{u}_{\mathcal{A}_\perp} \parallel \vec{e}_{\mathcal{A}_\perp}$ . Since we are minimizing  $G(\vec{u})$ , any strict inequality in  $\stackrel{(1)}{\geq}$  would mean that the right-hand collinear case produces a strictly smaller value of  $G(\vec{u})$ . Hence, no non-aligned  $\vec{u}$  can be optimal. At optimality,  $\stackrel{(1)}{\geq}$  must be tight and therefore  $\vec{u}^* \in \text{span}\{\vec{e}_{\mathcal{A}_\parallel}, \vec{e}_{\mathcal{A}_\perp}\}$ .  $\square$

**Proof of Proposition 2.** There are two edge cases where the **Problem (2)** degenerates into 1D.

**Case A** ( $\|\vec{e}_{\mathcal{A}_\parallel}\| = 0$  and  $\|\vec{e}_{\mathcal{A}_\perp}\| = 1$ ). This means  $\vec{e} = \vec{e}_{\mathcal{A}_\perp}$  is already fair. Then  $F$  becomes

$$F(\alpha, \beta) = w_1|\alpha| + w_2(1 - \beta).$$

Here, no debiasing is needed, and we set  $\alpha = 0$  and  $\beta = \|\vec{e}_{\mathcal{A}_\perp}\|$  to fully preserve utility, which gives  $\vec{u} = \vec{e} = \vec{e}_{\mathcal{A}_\perp}$  and  $\ell_{\text{self}} = 1 - \|\vec{e}_{\mathcal{A}_\perp}\| = 0$ .

**Case B** ( $\|\vec{e}_{\mathcal{A}_\perp}\| = 0$  and  $\|\vec{e}_{\mathcal{A}_\parallel}\| = 1$ ). This means  $\vec{e} = \vec{e}_{\mathcal{A}_\parallel}$  contains only attribute information (e.g., prompts like ‘‘a photo of a male’’ or ‘‘a photo of a female’’). In this case,  $F$  reduces to

$$F(\alpha) = w_1|\alpha| + w_2(1 - \alpha).$$

Since  $\vec{e}$  reflects purely attribute-related semantics, debiasing is unnecessary. Therefore, we fully preserve its utility by setting  $\alpha = \|\vec{e}_{\mathcal{A}_\parallel}\|, \beta = 0$ , which yields  $\vec{u} = \vec{e} = \vec{e}_{\mathcal{A}_\parallel}$  and  $\ell_{\text{self}} = 1 - \|\vec{e}_{\mathcal{A}_\parallel}\| = 0$ .  $\square$

**Proof of Lemma 2.** Assume  $\beta < 0$  and define a sign-flipped feasible point  $(\alpha, \tilde{\beta}) = (\alpha, -\beta)$ , where  $\tilde{\beta} > 0$ . The objective difference between the two points is

$$\begin{aligned} F(\alpha, \tilde{\beta}) - F(\alpha, \beta) &= w_1|\alpha| + w_2(1 - \alpha\|\vec{e}_{\mathcal{A}_\parallel}\| - \tilde{\beta}\|\vec{e}_{\mathcal{A}_\perp}\|) - \left[ w_1|\alpha| + w_2(1 - \alpha\|\vec{e}_{\mathcal{A}_\parallel}\| - \beta\|\vec{e}_{\mathcal{A}_\perp}\|) \right] \\ &= w_2(-\tilde{\beta}\|\vec{e}_{\mathcal{A}_\perp}\| + \beta\|\vec{e}_{\mathcal{A}_\perp}\|) \\ &= w_2(-(-\beta)\|\vec{e}_{\mathcal{A}_\perp}\| + \beta\|\vec{e}_{\mathcal{A}_\perp}\|) \\ &= 2w_2\beta\|\vec{e}_{\mathcal{A}_\perp}\| \\ &\stackrel{(1)}{\leq} 0. \end{aligned}$$

Here,  $\stackrel{(1)}{\leq}$  because  $w_2 \geq 0, \|\vec{e}_{\mathcal{A}_\perp}\| > 0$  and  $\beta < 0$ . Therefore,  $F(\alpha, \tilde{\beta}) \leq F(\alpha, \beta)$ , meaning that a negative  $\beta$  cannot yield a smaller objective value. Thus, the optimal solution must satisfy  $\beta \geq 0$ . A similar argument applies to  $\alpha$ . Assume  $\alpha < 0$  and define  $(\tilde{\alpha}, \beta) = (-\alpha, \beta)$ , where  $\tilde{\alpha} > 0$ . Then,

$$\begin{aligned} F(\tilde{\alpha}, \beta) - F(\alpha, \beta) &= w_1|\tilde{\alpha}| + w_2(1 - \tilde{\alpha}\|\vec{e}_{\mathcal{A}_\parallel}\| - \beta\|\vec{e}_{\mathcal{A}_\perp}\|) - \left[ w_1|\alpha| + w_2(1 - \alpha\|\vec{e}_{\mathcal{A}_\parallel}\| - \beta\|\vec{e}_{\mathcal{A}_\perp}\|) \right] \\ &\stackrel{(1)}{=} w_2 \left[ -\tilde{\alpha}\|\vec{e}_{\mathcal{A}_\parallel}\| + \alpha\|\vec{e}_{\mathcal{A}_\parallel}\| \right] \\ &= w_2 \left[ -(-\alpha)\|\vec{e}_{\mathcal{A}_\parallel}\| + \alpha\|\vec{e}_{\mathcal{A}_\parallel}\| \right] \\ &= 2w_2\alpha\|\vec{e}_{\mathcal{A}_\parallel}\| \\ &\stackrel{(2)}{\leq} 0. \end{aligned}$$

Here,  $\stackrel{(1)}{=}$  because  $|\tilde{\alpha}| = |-\alpha| = |\alpha|$  and  $\stackrel{(2)}{\leq}$  because  $w_2 \geq 0, \|\vec{e}_{\mathcal{A}_\parallel}\| > 0$  and  $\alpha < 0$ . Therefore, a negative  $\alpha$  also cannot provide a smaller objective value, implying that the optimal solution must satisfy  $\alpha \geq 0$ . Hence, all optimal solutions of **Problem (2)** lie in the first quadrant of the unit circle. We can then write the **Problem (2)** as

$$\min_{0 \leq \alpha \leq 1} F(\alpha) := w_1L(\alpha) + w_2V(\alpha),$$

where  $L(\alpha) = \alpha$  is the attribute leakage and  $V(\alpha) = 1 - \alpha \|\vec{e}_{\mathcal{A}_{\parallel}}\| - \sqrt{1 - \alpha^2} \|\vec{e}_{\mathcal{A}_{\perp}}\|$  is the self-utility loss.

We further show that no optimal solution can lie in the interval  $\|\vec{e}_{\mathcal{A}_{\parallel}}\| < \alpha \leq 1$ . Differentiating  $F(\alpha)$  gives

$$\frac{dF}{d\alpha} = w_1 \frac{dL}{d\alpha} + w_2 \frac{dV}{d\alpha} = w_1 + w_2 \frac{dV}{d\alpha}.$$

The derivative of  $V(\alpha)$  is

$$\frac{dV}{d\alpha} = -\frac{d}{d\alpha} \left( \alpha \|\vec{e}_{\mathcal{A}_{\parallel}}\| + \sqrt{1 - \alpha^2} \|\vec{e}_{\mathcal{A}_{\perp}}\| \right) = \frac{\alpha}{\sqrt{1 - \alpha^2}} \|\vec{e}_{\mathcal{A}_{\perp}}\| - \|\vec{e}_{\mathcal{A}_{\parallel}}\|. \quad (\alpha \neq 1)$$

Setting  $\frac{dV}{d\alpha} = 0$  yields

$$\frac{\alpha}{\sqrt{1 - \alpha^2}} = \frac{\|\vec{e}_{\mathcal{A}_{\parallel}}\|}{\|\vec{e}_{\mathcal{A}_{\perp}}\|} = \frac{\|\vec{e}_{\mathcal{A}_{\parallel}}\|}{\sqrt{1 - \|\vec{e}_{\mathcal{A}_{\parallel}}\|^2}}$$

The unique solution to this equation is  $\alpha = \|\vec{e}_{\mathcal{A}_{\parallel}}\|$ . To examine the sign of  $\frac{dV}{d\alpha}$  around this point, define the function  $h(x) = \frac{x}{\sqrt{1 - x^2}}$  on  $[0, 1)$ . Since

$$h'(x) = \frac{1}{(1 - x^2)^{3/2}} > 0 \quad \text{for } x \in [0, 1),$$

$h(x)$  is strictly increasing on  $[0, 1)$ . Consequently,

$$\alpha > \|\vec{e}_{\mathcal{A}_{\parallel}}\| \Rightarrow h(\alpha) > h(\|\vec{e}_{\mathcal{A}_{\parallel}}\|) \Rightarrow \frac{\alpha}{\sqrt{1 - \alpha^2}} > \frac{\|\vec{e}_{\mathcal{A}_{\parallel}}\|}{\sqrt{1 - \|\vec{e}_{\mathcal{A}_{\parallel}}\|^2}} \Rightarrow \frac{dV}{d\alpha} > 0,$$

and conversely,

$$\alpha < \|\vec{e}_{\mathcal{A}_{\parallel}}\| \Rightarrow h(\alpha) < h(\|\vec{e}_{\mathcal{A}_{\parallel}}\|) \Rightarrow \frac{\alpha}{\sqrt{1 - \alpha^2}} < \frac{\|\vec{e}_{\mathcal{A}_{\parallel}}\|}{\sqrt{1 - \|\vec{e}_{\mathcal{A}_{\parallel}}\|^2}} \Rightarrow \frac{dV}{d\alpha} < 0,$$

Since  $w_1, w_2 \geq 0$  and  $w_1 + w_2 = 1$ , when  $\alpha > \|\vec{e}_{\mathcal{A}_{\parallel}}\|$ , it follows that

$$\frac{dF}{d\alpha} = w_1 + w_2 \frac{dV}{d\alpha} > 0$$

Hence,  $F(\alpha)$  is strictly increasing on  $(\|\vec{e}_{\mathcal{A}_{\parallel}}\|, 1)$  and cannot achieve an optimum in this interval. Next, we examine the boundary case  $\alpha = 1$ . At  $\alpha = 1$ , we have  $F(1) = w_1 + w_2(1 - \|\vec{e}_{\mathcal{A}_{\parallel}}\|)$ . At  $\alpha = \|\vec{e}_{\mathcal{A}_{\parallel}}\|$ , we have  $F(\|\vec{e}_{\mathcal{A}_{\parallel}}\|) = w_1 \|\vec{e}_{\mathcal{A}_{\parallel}}\|$ . The difference between these two values is

$$F(1) - F(\|\vec{e}_{\mathcal{A}_{\parallel}}\|) = w_1(1 - \|\vec{e}_{\mathcal{A}_{\parallel}}\|) + w_2(1 - \|\vec{e}_{\mathcal{A}_{\parallel}}\|) \geq 0,$$

which confirms that  $F(1) \geq F(\|\vec{e}_{\mathcal{A}_{\parallel}}\|)$ . Thus, we can conclude that all optimal solutions must satisfy  $0 \leq \alpha \leq \|\vec{e}_{\mathcal{A}_{\parallel}}\|$ .

Within this feasible range, we have  $\frac{dL}{d\alpha} = 1 > 0$  and  $\frac{dV}{d\alpha} \leq 0$ , implying that  $L(\alpha)$  is strictly increasing while  $V(\alpha)$  is strictly decreasing on  $[0, \|\vec{e}_{\mathcal{A}_{\parallel}}\|]$ . For any two feasible points  $\alpha_1 < \alpha_2 \leq \|\vec{e}_{\mathcal{A}_{\parallel}}\|$ , it follows that  $L(\alpha_1) < L(\alpha_2)$  and  $V(\alpha_1) > V(\alpha_2)$ , indicating that reducing leakage necessarily increasing self-utility loss. Each  $\alpha$  in this interval thus yields a distinct non-dominated pair  $(L(\alpha), V(\alpha))$ . Therefore, the set  $\alpha \in [0, \|\vec{e}_{\mathcal{A}_{\parallel}}\|]$  fully characterizes the Pareto front.  $\square$

**Proof of Theorem 1.** For any scalars  $(x, y)$  and weights  $(w_1, w_2) \in \Delta := \{w_1, w_2 \geq 0, w_1 + w_2 = 1\}$ , we have

$$\sup_{(w_1, w_2) \in \Delta} (w_1 x + w_2 y) = \max\{x, y\}.$$

Therefore, the **Problem (3)** yields the following minimax formulation:

$$\min_{0 \leq \alpha \leq \|\vec{e}_{\mathcal{A}_{\parallel}}\|} \sup_{\substack{w_1, w_2 \geq 0 \\ w_1 + w_2 = 1}} \left\{ w_1 L(\alpha) + w_2 V(\alpha) \right\} = \min_{0 \leq \alpha \leq \|\vec{e}_{\mathcal{A}_{\parallel}}\|} \max\{L(\alpha), V(\alpha)\}$$

Since the two loss functions operate on different numerical scales over  $\alpha \in [0, \|\vec{e}_{\mathcal{A}_{\parallel}}\|]$ , we normalize each to the interval  $[0, 1]$ :

$$\tilde{L}(\alpha) = \frac{\alpha}{\|\vec{e}_{\mathcal{A}_{\parallel}}\|}, \quad \tilde{V}(\alpha) = \frac{1 - (\sqrt{1 - \alpha^2} \|\vec{e}_{\mathcal{A}_{\perp}}\| + \alpha \|\vec{e}_{\mathcal{A}_{\parallel}}\|)}{1 - \|\vec{e}_{\mathcal{A}_{\perp}}\|}.$$

This normalization ensures that  $\tilde{L}(0) = 0$ ,  $\tilde{L}(\|\vec{e}_{\mathcal{A}_{\parallel}}\|) = 1$ , and  $\tilde{V}(0) = 1$ ,  $\tilde{V}(\|\vec{e}_{\mathcal{A}_{\parallel}}\|) = 0$ . Hence, **Problem (3)** becomes

$$\min_{0 \leq \alpha \leq \|\vec{e}_{\mathcal{A}_{\parallel}}\|} \max\{\tilde{L}(\alpha), \tilde{V}(\alpha)\}$$

By **Lemma 2**, over the interval  $[0, \|\vec{e}_{\mathcal{A}_{\parallel}}\|]$ ,  $\tilde{L}(\alpha)$  is strictly increasing while  $\tilde{V}(\alpha)$  is strictly decreasing. Therefore,  $\max\{\tilde{L}, \tilde{V}\}$  is minimized *uniquely* at the point where they intersect:

$$\tilde{L}(\alpha^*) = \tilde{V}(\alpha^*) \iff \frac{\alpha^*}{\|\vec{e}_{\mathcal{A}_{\parallel}}\|} = \frac{1 - (\sqrt{1 - (\alpha^*)^2} \|\vec{e}_{\mathcal{A}_{\perp}}\| + \alpha^* \|\vec{e}_{\mathcal{A}_{\parallel}}\|)}{1 - \|\vec{e}_{\mathcal{A}_{\perp}}\|}.$$

Rearranging, we obtain

$$\|\vec{e}_{\mathcal{A}_{\perp}}\| \sqrt{1 - (\alpha^*)^2} = 1 - \alpha^* \left( \|\vec{e}_{\mathcal{A}_{\parallel}}\| + \frac{1 - \|\vec{e}_{\mathcal{A}_{\perp}}\|}{\|\vec{e}_{\mathcal{A}_{\parallel}}\|} \right).$$

For this equality to hold, the right-hand side must be positive, which provides an upper bound on  $\alpha^*$ :

$$\alpha^* < \frac{1}{\|\vec{e}_{\mathcal{A}_{\parallel}}\| + \frac{1 - \|\vec{e}_{\mathcal{A}_{\perp}}\|}{\|\vec{e}_{\mathcal{A}_{\parallel}}\|}}. \quad (\text{C2})$$

Squaring both sides (as both are nonnegative) yields

$$\|\vec{e}_{\mathcal{A}_{\perp}}\|^2 (1 - (\alpha^*)^2) = \left( 1 - \alpha^* \left( \|\vec{e}_{\mathcal{A}_{\parallel}}\| + \frac{1 - \|\vec{e}_{\mathcal{A}_{\perp}}\|}{\|\vec{e}_{\mathcal{A}_{\parallel}}\|} \right) \right)^2.$$

Expanding and rearranging leads to a quadratic in  $\alpha^*$ :

$$Q(\alpha^*) := \left( \left( \|\vec{e}_{\mathcal{A}_{\parallel}}\| + \frac{1 - \|\vec{e}_{\mathcal{A}_{\perp}}\|}{\|\vec{e}_{\mathcal{A}_{\parallel}}\|} \right)^2 + \|\vec{e}_{\mathcal{A}_{\perp}}\|^2 \right) (\alpha^*)^2 - 2 \left( \|\vec{e}_{\mathcal{A}_{\parallel}}\| + \frac{1 - \|\vec{e}_{\mathcal{A}_{\perp}}\|}{\|\vec{e}_{\mathcal{A}_{\parallel}}\|} \right) \alpha^* + \|\vec{e}_{\mathcal{A}_{\parallel}}\|^2 = 0.$$

The discriminant is

$$\begin{aligned} \Delta &= 4 \left[ \left( \|\vec{e}_{\mathcal{A}_{\parallel}}\| + \frac{1 - \|\vec{e}_{\mathcal{A}_{\perp}}\|}{\|\vec{e}_{\mathcal{A}_{\parallel}}\|} \right)^2 - \left( \left( \|\vec{e}_{\mathcal{A}_{\parallel}}\| + \frac{1 - \|\vec{e}_{\mathcal{A}_{\perp}}\|}{\|\vec{e}_{\mathcal{A}_{\parallel}}\|} \right)^2 + \|\vec{e}_{\mathcal{A}_{\perp}}\|^2 \right) \|\vec{e}_{\mathcal{A}_{\parallel}}\|^2 \right] \\ &= 4 \left[ (1 - \|\vec{e}_{\mathcal{A}_{\parallel}}\|^2) \left( \|\vec{e}_{\mathcal{A}_{\parallel}}\| + \frac{1 - \|\vec{e}_{\mathcal{A}_{\perp}}\|}{\|\vec{e}_{\mathcal{A}_{\parallel}}\|} \right)^2 - \|\vec{e}_{\mathcal{A}_{\perp}}\|^2 \|\vec{e}_{\mathcal{A}_{\parallel}}\|^2 \right] \\ &= 4 \|\vec{e}_{\mathcal{A}_{\perp}}\|^2 \left[ \left( \|\vec{e}_{\mathcal{A}_{\parallel}}\| + \frac{1 - \|\vec{e}_{\mathcal{A}_{\perp}}\|}{\|\vec{e}_{\mathcal{A}_{\parallel}}\|} \right)^2 - \|\vec{e}_{\mathcal{A}_{\parallel}}\|^2 \right] \\ &= 4 \|\vec{e}_{\mathcal{A}_{\perp}}\|^2 \left( \frac{(1 - \|\vec{e}_{\mathcal{A}_{\perp}}\|)^2}{\|\vec{e}_{\mathcal{A}_{\parallel}}\|^2} + 2(1 - \|\vec{e}_{\mathcal{A}_{\perp}}\|) \right) \\ &> 0 \end{aligned}$$

Thus, there exist two real roots:

$$\alpha_{\pm} = \frac{\left( \|\vec{e}_{\mathcal{A}_{\parallel}}\| + \frac{1 - \|\vec{e}_{\mathcal{A}_{\perp}}\|}{\|\vec{e}_{\mathcal{A}_{\parallel}}\|} \right) \pm \|\vec{e}_{\mathcal{A}_{\perp}}\| \sqrt{\left( \|\vec{e}_{\mathcal{A}_{\parallel}}\| + \frac{1 - \|\vec{e}_{\mathcal{A}_{\perp}}\|}{\|\vec{e}_{\mathcal{A}_{\parallel}}\|} \right)^2 - \|\vec{e}_{\mathcal{A}_{\parallel}}\|^2}}{\left( \|\vec{e}_{\mathcal{A}_{\parallel}}\| + \frac{1 - \|\vec{e}_{\mathcal{A}_{\perp}}\|}{\|\vec{e}_{\mathcal{A}_{\parallel}}\|} \right)^2 + \|\vec{e}_{\mathcal{A}_{\perp}}\|^2}$$

Since the solution is unique, we need to verify which root satisfies the feasibility conditions.

Let

$$E := \|\vec{e}_{\mathcal{A}_{\parallel}}\| + \frac{1 - \|\vec{e}_{\mathcal{A}_{\perp}}\|}{\|\vec{e}_{\mathcal{A}_{\parallel}}\|}, \quad \text{so that} \quad \alpha_+ = \frac{E + \|\vec{e}_{\mathcal{A}_{\perp}}\| \sqrt{E^2 - \|\vec{e}_{\mathcal{A}_{\parallel}}\|^2}}{E^2 + \|\vec{e}_{\mathcal{A}_{\perp}}\|^2}.$$

The feasibility conditions are:

$$(C1) \quad 0 < \alpha^* < \|\vec{e}_{\mathcal{A}_{\parallel}}\|, \quad (C2) \quad \alpha^* < \frac{1}{E}.$$

We show that  $\alpha_+$  violates at least one of these conditions.

**Case A:**  $E \geq 1$ . Consider

$$\alpha_+ - \frac{1}{E} = \frac{E + \|\vec{e}_{\mathcal{A}_{\perp}}\| \sqrt{E^2 - \|\vec{e}_{\mathcal{A}_{\parallel}}\|^2}}{E^2 + \|\vec{e}_{\mathcal{A}_{\perp}}\|^2} - \frac{1}{E} = \frac{\|\vec{e}_{\mathcal{A}_{\perp}}\| (E \sqrt{E^2 - \|\vec{e}_{\mathcal{A}_{\parallel}}\|^2} - \|\vec{e}_{\mathcal{A}_{\perp}}\|)}{E(E^2 + \|\vec{e}_{\mathcal{A}_{\perp}}\|^2)}.$$

The denominator is positive. For the numerator, since  $E \geq 1$ , we have

$$(E \sqrt{E^2 - \|\vec{e}_{\mathcal{A}_{\parallel}}\|^2})^2 - \|\vec{e}_{\mathcal{A}_{\perp}}\|^2 = (E^2 - \|\vec{e}_{\mathcal{A}_{\parallel}}\|^2)E^2 - \|\vec{e}_{\mathcal{A}_{\perp}}\|^2 = (E^2 - 1)(E^2 + \|\vec{e}_{\mathcal{A}_{\perp}}\|^2) \geq 0,$$

Hence,

$$(E \sqrt{E^2 - \|\vec{e}_{\mathcal{A}_{\parallel}}\|^2})^2 - \|\vec{e}_{\mathcal{A}_{\perp}}\|^2 = \left( E \sqrt{E^2 - \|\vec{e}_{\mathcal{A}_{\parallel}}\|^2} - \|\vec{e}_{\mathcal{A}_{\perp}}\| \right) \left( E \sqrt{E^2 - \|\vec{e}_{\mathcal{A}_{\parallel}}\|^2} + \|\vec{e}_{\mathcal{A}_{\perp}}\| \right) \geq 0.$$

Since  $E \sqrt{E^2 - \|\vec{e}_{\mathcal{A}_{\parallel}}\|^2} + \|\vec{e}_{\mathcal{A}_{\perp}}\| \geq 0$ , we have

$$E \sqrt{E^2 - \|\vec{e}_{\mathcal{A}_{\parallel}}\|^2} - \|\vec{e}_{\mathcal{A}_{\perp}}\| \geq 0 \implies \alpha_+ - \frac{1}{E} \geq 0.$$

Thus,  $\alpha_+$  violates (C2) when  $E \geq 1$ , making it infeasible.

**Case B:**  $E < 1$ . From  $E = \|\vec{e}_{\mathcal{A}_{\parallel}}\| + \frac{1 - \|\vec{e}_{\mathcal{A}_{\perp}}\|}{\|\vec{e}_{\mathcal{A}_{\parallel}}\|} < 1$  with  $\|\vec{e}_{\mathcal{A}_{\parallel}}\|^2 + \|\vec{e}_{\mathcal{A}_{\perp}}\|^2 = 1$ , we deduce

$$1 - \|\vec{e}_{\mathcal{A}_{\perp}}\| < \|\vec{e}_{\mathcal{A}_{\parallel}}\|(1 - \|\vec{e}_{\mathcal{A}_{\perp}}\|) \leq \frac{1}{4} \implies \|\vec{e}_{\mathcal{A}_{\perp}}\| \geq \frac{3}{4} > \frac{1}{2}.$$

Evaluating  $Q(\alpha^*)$  at  $\alpha^* = \|\vec{e}_{\mathcal{A}_{\parallel}}\|$  gives

$$\begin{aligned} Q(\|\vec{e}_{\mathcal{A}_{\parallel}}\|) &= \left( \left( \|\vec{e}_{\mathcal{A}_{\parallel}}\| + \frac{1 - \|\vec{e}_{\mathcal{A}_{\perp}}\|}{\|\vec{e}_{\mathcal{A}_{\parallel}}\|} \right)^2 + \|\vec{e}_{\mathcal{A}_{\perp}}\|^2 \right) \|\vec{e}_{\mathcal{A}_{\parallel}}\|^2 - 2 \left( \|\vec{e}_{\mathcal{A}_{\parallel}}\| + \frac{1 - \|\vec{e}_{\mathcal{A}_{\perp}}\|}{\|\vec{e}_{\mathcal{A}_{\parallel}}\|} \right) \|\vec{e}_{\mathcal{A}_{\parallel}}\| + \|\vec{e}_{\mathcal{A}_{\parallel}}\|^2 \\ &= \left( \|\vec{e}_{\mathcal{A}_{\parallel}}\| + \frac{1 - \|\vec{e}_{\mathcal{A}_{\perp}}\|}{\|\vec{e}_{\mathcal{A}_{\parallel}}\|} \right)^2 \|\vec{e}_{\mathcal{A}_{\parallel}}\|^2 + \|\vec{e}_{\mathcal{A}_{\perp}}\|^2 \|\vec{e}_{\mathcal{A}_{\parallel}}\|^2 - 2 \left( \|\vec{e}_{\mathcal{A}_{\parallel}}\|^2 + 1 - \|\vec{e}_{\mathcal{A}_{\perp}}\| \right) + \|\vec{e}_{\mathcal{A}_{\parallel}}\|^2 \\ &= \left[ \|\vec{e}_{\mathcal{A}_{\parallel}}\|^4 + 2(1 - \|\vec{e}_{\mathcal{A}_{\perp}}\|) \|\vec{e}_{\mathcal{A}_{\parallel}}\|^2 + (1 - \|\vec{e}_{\mathcal{A}_{\perp}}\|)^2 \right] + \|\vec{e}_{\mathcal{A}_{\perp}}\|^2 \|\vec{e}_{\mathcal{A}_{\parallel}}\|^2 - 2 \left( \|\vec{e}_{\mathcal{A}_{\parallel}}\|^2 + 1 - \|\vec{e}_{\mathcal{A}_{\perp}}\| \right) + \|\vec{e}_{\mathcal{A}_{\parallel}}\|^2 \\ &= \|\vec{e}_{\mathcal{A}_{\parallel}}\|^4 + \left( 2(1 - \|\vec{e}_{\mathcal{A}_{\perp}}\|) + \|\vec{e}_{\mathcal{A}_{\perp}}\|^2 - 1 \right) \|\vec{e}_{\mathcal{A}_{\parallel}}\|^2 + \left( (1 - \|\vec{e}_{\mathcal{A}_{\perp}}\|)^2 - 2(1 - \|\vec{e}_{\mathcal{A}_{\perp}}\|) \right) \\ &= \|\vec{e}_{\mathcal{A}_{\parallel}}\|^4 + (\|\vec{e}_{\mathcal{A}_{\perp}}\|^2 - 2\|\vec{e}_{\mathcal{A}_{\perp}}\| + 1) \|\vec{e}_{\mathcal{A}_{\parallel}}\|^2 + (\|\vec{e}_{\mathcal{A}_{\perp}}\|^2 - 1) \\ &= \|\vec{e}_{\mathcal{A}_{\parallel}}\|^4 + ((1 - \|\vec{e}_{\mathcal{A}_{\perp}}\|)^2 - 2\|\vec{e}_{\mathcal{A}_{\perp}}\| + 1) \|\vec{e}_{\mathcal{A}_{\parallel}}\|^2 + ((1 - \|\vec{e}_{\mathcal{A}_{\perp}}\|)^2 - 1) \\ &= \|\vec{e}_{\mathcal{A}_{\parallel}}\|^4 + (2 - 2\|\vec{e}_{\mathcal{A}_{\perp}}\| - \|\vec{e}_{\mathcal{A}_{\perp}}\|^2) \|\vec{e}_{\mathcal{A}_{\parallel}}\|^2 - \|\vec{e}_{\mathcal{A}_{\perp}}\|^2 \\ &= \|\vec{e}_{\mathcal{A}_{\parallel}}\|^4 + (2 - 2\|\vec{e}_{\mathcal{A}_{\perp}}\|) \|\vec{e}_{\mathcal{A}_{\parallel}}\|^2 - \|\vec{e}_{\mathcal{A}_{\perp}}\|^4 - \|\vec{e}_{\mathcal{A}_{\parallel}}\|^2 \\ &= \|\vec{e}_{\mathcal{A}_{\parallel}}\|^2 (1 - 2\|\vec{e}_{\mathcal{A}_{\perp}}\|) \\ &< 0 \quad (\text{since } \|\vec{e}_{\mathcal{A}_{\perp}}\| > \frac{1}{2}), \end{aligned}$$

Because the quadratic coefficient  $E^2 + \|\vec{e}_{\mathcal{A}_\perp}\|^2 > 0$ , one root lies below  $\|\vec{e}_{\mathcal{A}_\parallel}\|$  and the other lies strictly above it. The larger root corresponds to  $\alpha_+$ , so

$$\alpha_+ > \|\vec{e}_{\mathcal{A}_\parallel}\|,$$

which violates (C1). Therefore,  $\alpha_+$  is infeasible also when  $E < 1$ .

Combining **Cases A** and **B**, the  $\alpha_+$  can never simultaneously satisfies both (C1) and (C2).

Therefore,

$$\alpha^* := \alpha_- = \frac{\left(\|\vec{e}_{\mathcal{A}_\parallel}\| + \frac{1 - \|\vec{e}_{\mathcal{A}_\perp}\|}{\|\vec{e}_{\mathcal{A}_\parallel}\|}\right) - \|\vec{e}_{\mathcal{A}_\perp}\| \sqrt{\left(\|\vec{e}_{\mathcal{A}_\parallel}\| + \frac{1 - \|\vec{e}_{\mathcal{A}_\perp}\|}{\|\vec{e}_{\mathcal{A}_\parallel}\|}\right)^2 - \|\vec{e}_{\mathcal{A}_\parallel}\|^2}}{\left(\|\vec{e}_{\mathcal{A}_\parallel}\| + \frac{1 - \|\vec{e}_{\mathcal{A}_\perp}\|}{\|\vec{e}_{\mathcal{A}_\parallel}\|}\right)^2 + \|\vec{e}_{\mathcal{A}_\perp}\|^2}.$$

The optimal debiased embedding is

$$\vec{u}^* = \sqrt{1 - (\alpha^*)^2} \frac{\vec{e}_{\mathcal{A}_\perp}}{\|\vec{e}_{\mathcal{A}_\perp}\|} + \alpha^* \frac{\vec{e}_{\mathcal{A}_\parallel}}{\|\vec{e}_{\mathcal{A}_\parallel}\|}.$$

The attribute leakage and self-utility loss at  $\vec{u}^*$  are given by

$$L(\alpha^*) = \alpha^* \quad \text{and} \quad \tilde{L}(\alpha^*) = \tilde{V}(\alpha^*) \implies \frac{\alpha^*}{\|\vec{e}_{\mathcal{A}_\parallel}\|} = \frac{V(\alpha^*)}{1 - \|\vec{e}_{\mathcal{A}_\perp}\|} \implies V(\alpha^*) = (1 - \|\vec{e}_{\mathcal{A}_\perp}\|) \frac{\alpha^*}{\|\vec{e}_{\mathcal{A}_\parallel}\|}.$$

Finally, by **Proposition 1**, we have a tighter upper bound on the cross-utility loss as:

$$\ell_{\text{cross}} \leq \sqrt{2(1 - \|\vec{e}_{\mathcal{A}_\perp}^{(I)}\|) \frac{\alpha^*}{\|\vec{e}_{\mathcal{A}_\parallel}^{(I)}\|}} + \sqrt{2(1 - \|\vec{e}_{\mathcal{A}_\perp}^{(T)}\|) \frac{\alpha^*}{\|\vec{e}_{\mathcal{A}_\parallel}^{(T)}\|}} \leq \sqrt{2(1 - \|\vec{e}_{\mathcal{A}_\perp}^{(I)}\|)} + \sqrt{2(1 - \|\vec{e}_{\mathcal{A}_\perp}^{(T)}\|)}$$

□

## B. Details of LLM

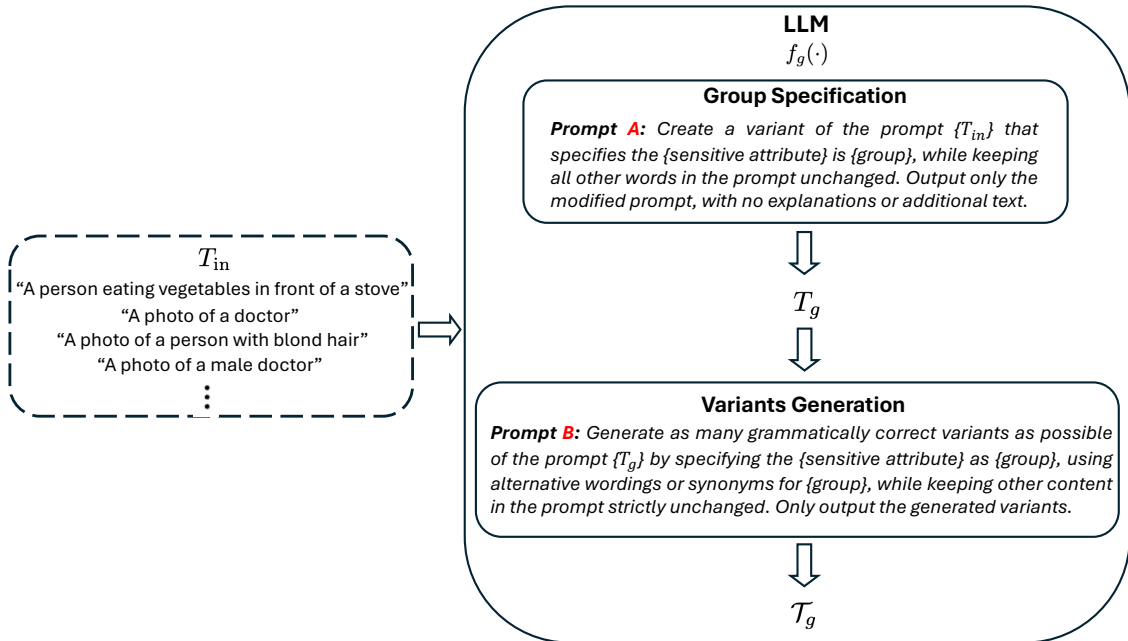


Figure 5. An illustration of the prompts we use in an LLM to insert the group specification and generate the variants for each group  $g$ .

As shown in Fig. 1, this module is template agnostic. The input prompt can take any form, whether neutral or group-specific, and all follow the same process. Once a sensitive attribute and its groups are defined, an LLM  $f_g(\cdot)$  is used for each group to generate prompts. For each group, we collect the group-specific prompt  $T_g$  and its variants  $\mathcal{T}_g$ , which are then fed into the text encoder of a VLM as described in Section 4.1 of the main paper. As shown in Fig. 2 and Fig. 3, we provide several examples of the LLM inputs and outputs.

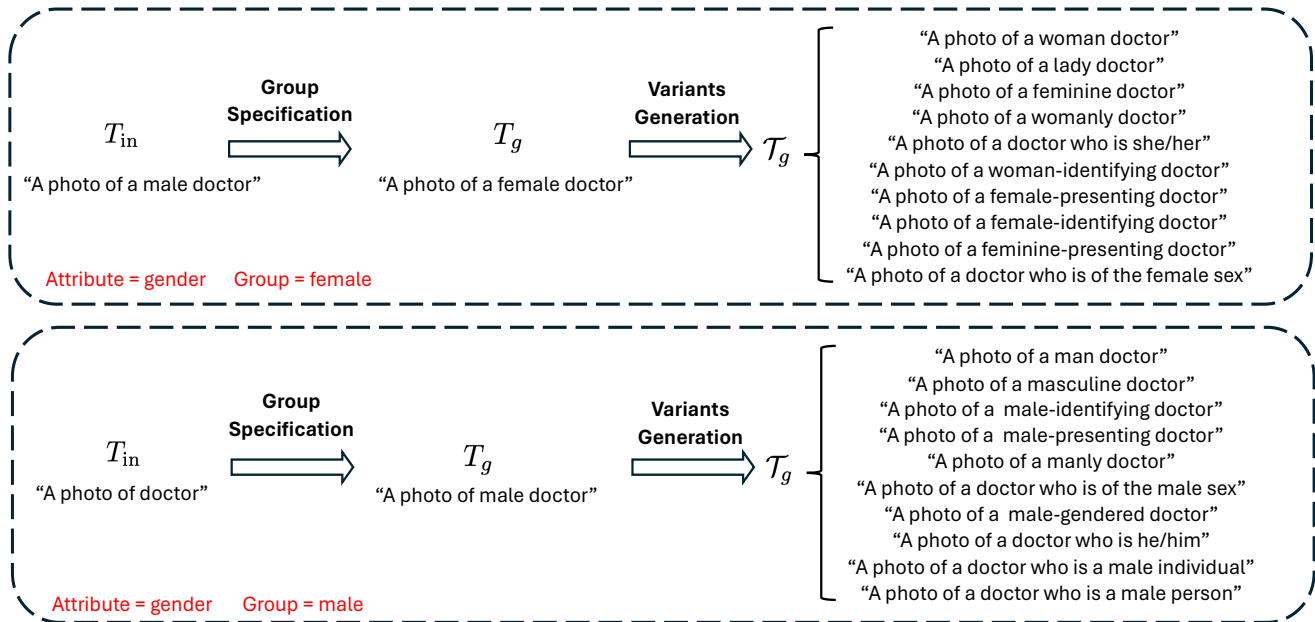


Figure 6. An illustration of the LLM output when the input is group-specific/neutral. The sensitive attribute is gender, and the selected group is female/male.

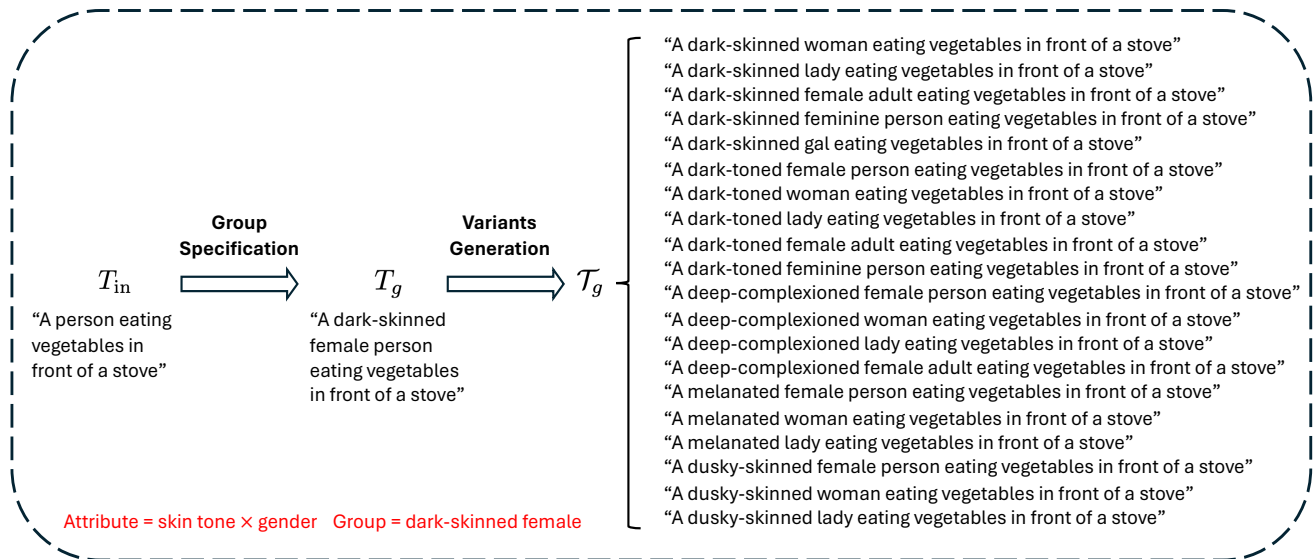


Figure 7. An illustration of the LLM output when the input is neutral. The sensitive attribute is the intersection of skin tone and gender, and the selected group is dark-skinned female.

## C. Prompts in Text-to-Image Generation

We use the following 34 occupations: *doctor, aerospace engineer, computer programmer, electrical engineer, scientist, artist, designer, musician, painter, photographer, singer, writer, architect, civil engineer, engineer, software developer, childcare worker, coach, dentist, clerk, housekeeper, massage therapist, nurse, psychologist, social worker, teacher, professor, CEO, skateboarder, surfer, baseball player, football player, soccer player, tennis player.*

The occupation list is adapted from [8, 14] with several modifications for clarity and redundancy reduction. Specifically, we remove *maid* as it is inherently gendered, and delete *dental assistant* and *dental hygienist* due to their similarity to *dentist*. We also exclude *programmer* since *computer programmer* is already included, and remove *therapist* as it overlaps with *massage therapist*. Additionally, *author* is omitted because *writer* serves the same purpose, and *social assistant* is excluded due to the presence of *social worker*.

We then use these 34 occupations to create prompts following the template “a photo of a/an occupation.” As shown in Fig. 4, this results in 34 neutral prompts for fairness evaluation. We also construct 34 group-explicit prompts to evaluate utility. For each occupation, the group-explicit prompt specifies the gender group that the original model is biased toward. This choice is intentional, as many debiasing methods tend to overcorrect and fail to generate images for the originally dominant group once debiased. For example, the original SD model tends to generate male images for the occupation *doctor*, while the debiased model balances the gender distribution but often struggles to generate male images when explicitly prompted, as it has been adjusted to produce more female representations.

Fairness		Utility	
A photo of a doctor	A photo of a coach	A photo of a male doctor	A photo of a male coach
A photo of an aerospace engineer	A photo of a dentist	A photo of a male aerospace engineer	A photo of a male dentist
A photo of a computer programmer	A photo of a clerk	A photo of a male computer programmer	A photo of a female clerk
A photo of an electrical engineer	A photo of a housekeeper	A photo of a male electrical engineer	A photo of a female housekeeper
A photo of a scientist	A photo of a massage therapist	A photo of a male scientist	A photo of a female massage therapist
A photo of an artist	A photo of a nurse	A photo of a female artist	A photo of a female nurse
A photo of a designer	A photo of a psychologist	A photo of a female designer	A photo of a female psychologist
A photo of a musician	A photo of a social worker	A photo of a male musician	A photo of a female social worker
A photo of a painter	A photo of a teacher	A photo of a female painter	A photo of a female teacher
A photo of a photographer	A photo of a professor	A photo of a female photographer	A photo of a male professor
A photo of a singer	A photo of a CEO	A photo of a female singer	A photo of a male CEO
A photo of a writer	A photo of a skateboarder	A photo of a male writer	A photo of a male skateboarder
A photo of an architect	A photo of a surfer	A photo of a male architect	A photo of a male surfer
A photo of a civil engineer	A photo of a baseball player	A photo of a male civil engineer	A photo of a male baseball player
A photo of an engineer	A photo of a football player	A photo of a male engineer	A photo of a male football player
A photo of a software developer	A photo of a soccer player	A photo of a male software developer	A photo of a male soccer player
A photo of a childcare worker	A photo of a tennis player	A photo of a female childcare worker	A photo of a female tennis player

Figure 8. An illustration of neutral prompts used for fairness evaluation and group-explicit prompts used for utility evaluation in the text-to-image generation task.

## D. Evaluations of Text-to-Image Generation

For the **fairness evaluation**, we use 34 neutral prompts. For each prompt, we generate 100 images using five models: the original SD, Orth-Proj, Orth-Cali, SFID, and ours, resulting in a total of **17,000 generated images**. For quantitative evaluation, we query BLIP-2 with the question: “What is the perceived gender of the person in this image?” and compute  $\overline{SP}_{\mathcal{T}_o}$  based on BLIP-2’s annotations. For qualitative evaluation, we select the top-5 prompts  $\mathcal{T}_o^5 \subset \mathcal{T}_o$  showing the highest  $SP_t$  scores under the original SD model: “A photo of a doctor,” “A photo of a CEO,” “A photo of a computer programmer,” “A photo of a designer,” and “A photo of a civil engineer.” Each prompt has 100 generated images per model, totaling **2,500 images** for manual inspection. Three independent annotators answer the same question asked of BLIP-2 with three options: *male*, *female*, or *unsure*. Images labeled as *unsure* or with disagreement among annotators are regenerated until unanimous agreement is reached. As a result, all analyzed images have unanimously agreed perceived gender labels (male or female).

For the **utility evaluation**, we use 34 group-explicit prompts. Again, 100 images are generated per prompt for each of the five models, resulting in another **17,000 images**. For quantitative evaluation, we compute the CLIP score to measure image–text alignment and report the average score across all 34 prompts. For qualitative evaluation, we select the top-5 prompts with the lowest CLIP scores under the original SD model: “A photo of a male electrical engineer,” “A photo of a female photographer,” “A photo of a male professor,” “A photo of a male dentist,” and “A photo of a male football player.”

Each prompt produces 100 images per model, totaling **2,500 images** for manual inspection. The same three annotators identify images where the perceived gender does not match the one specified in the prompt. The number of mismatched images is denoted as  $N_I$ , and the *generation accuracy* is computed as  $\text{Acc}^G = (N_G - N_I)/N_G$ , where  $N_G = 500$  is the total number of images per prompt. Images labeled as *unsure* or with non-unanimous annotations are regenerated until full agreement is reached, ensuring that all final images have unanimously agreed perceived gender labels.

**Ethical Statement.** We do not collect any personal information from the annotators, and all annotations are performed exclusively on AI-generated images. No personal data of real human subjects is involved in this study.

## E. Datasets

**CelebA.** The CelebA is a binary facial attribute public dataset widely used as a benchmark for fairness evaluation in computer vision. It consists of facial attribute images, and we use its original validation and test sets, totaling 39,829 images for both utility and fairness evaluation.

**FACET.** The FACET dataset is a publicly available benchmark created by Meta AI for evaluating fairness in computer vision. It contains approximately 32,000 images, each annotated with various attributes, including perceived gender, age, and skin tone. The original dataset provides bounding boxes for each person. By cropping each individual from the original images, we obtain 49,550 single-person images. For our experiments, we use perceived gender as the sensitive attribute. To maintain consistency with previous debiasing studies [5, 21], we exclude samples labeled as non-binary or unsure. The dataset also includes 52 occupation classes, which serve as the classification labels. To ensure statistically reliable results, we remove classes with fewer than 1000 samples, resulting in 26,834 images across 18 occupation categories. The retained occupations are: *lawman, laborer, boatman, basketball\_player, tennis\_player, backpacker, speaker, soldier, farmer, guard, dancer, singer, ballplayer, soccer\_player, repairman, guitarist, seller, motorcyclist*.

**Flickr30K.** Flickr30K is a public image–caption dataset containing 31,783 real-world images, each paired with up to five human-written descriptive sentences, resulting in a total of 158,915 image–text pairs. We first use YOLOv8 [20] to select images containing only one person. For these selected images, we retain captions that include gender-explicit words from the list [*"man", "woman", "boy", "girl", "gentleman", "guy", "lady", "female", "male"*]. Captions containing any of [*"man", "boy", "gentleman", "guy", "male"*] are labeled as *male*, while those with [*"woman", "girl", "lady", "female"*] are labeled as *female*. After filtering, we obtain 3,079 image–text pairs for the retrieval task. To evaluate fairness, we further modify the captions by replacing gender-explicit words with the neutral term "*person*", and these neutralized captions are used as text queries.

**COCO2017.** The COCO2017 dataset is one of the most widely used image–caption datasets in computer vision, containing five human-written captions per image. We use a subset of the original training and validation sets provided by [52], which includes explicit annotations for perceived gender and skin tone. These annotations were collected by multiple annotators using a more rigorous and reliable labeling protocol. In total, 28,316 images were annotated. We further exclude samples where either the perceived gender or skin tone is labeled as unsure, resulting in 1,368 image–text pairs. Similar to Flickr30K, to evaluate fairness, we modify the captions by replacing gender-explicit words with the neutral term "*person*", and use these neutralized captions as text queries.

## F. Results of Other VLMs

Table 6. Experimental results of CLIP (ResNet50) on the zero-shot image classification task.

Datasets	CelebA			FACET		
Evaluation Metric	F1 $\uparrow$	$\Delta_{EO}^{Avg}$ (G×A) $\downarrow$	$\Delta_{EO}^{Max}$ (G×A) $\downarrow$	Macro F1 $\uparrow$	$\Delta_{EO}^{Avg}$ (G) $\downarrow$	$\Delta_{EO}^{Max}$ (G) $\downarrow$
Baseline CLIP (ResNet50)	60.7±0.5	15.3±0.3	30.0±0.4	59.2±0.2	9.3±0.6	48.9±0.1
✓  I&T SFID	56.4±0.2	14.6±0.5	24.9±0.3	[50.8]±0.6	9.4±0.4	47.2±0.2
✓  I&T FairerCLIP	[56.6]±0.3	14.2±0.1	<b>[21.4]</b> ±0.4	50.7±0.5	8.9±0.6	47.2±0.2
✗  I&T PRISM	56.3±0.1	14.7±0.4	[21.8]±0.3	50.5±0.6	<b>[8.4]</b> ±0.5	47.6±0.2
✗  I&T PRISM-mini	56.0±0.6	13.7±0.3	24.9±0.1	49.2±0.4	8.9±0.5	46.6±0.2
✗  I&T RoboShot	55.8±0.4	<b>[10.9]</b> ±0.2	<b>[21.4]</b> ±0.3	50.7±0.1	9.0±0.6	<b>[45.6]</b> ±0.5
✗  T Orth-Proj	56.4±0.3	14.6±0.5	24.4±0.2	47.8±0.6	8.8±0.4	47.9±0.1
✗  T Orth-Cali	55.6±0.2	14.5±0.4	24.5±0.3	49.6±0.6	8.9±0.1	47.6±0.5
✗  I&T Ours	<b>[58.5]</b> ±0.4	[11.5]±0.3	[21.8]±0.2	<b>[58.6]</b> ±0.1	[8.5]±0.2	[45.8]±0.5

Table 7. Experimental results of CLIP (ResNet50) on the text-to-image retrieval task.

Datasets	COCO2017			Flickr30K		
Evaluation Metric	R@5 $\uparrow$	R@10 $\uparrow$	MS@1000 (G×ST) $\downarrow$	R@5 $\uparrow$	R@10 $\uparrow$	MS@1000 (G) $\downarrow$
Baseline CLIP (ResNet50)	71.4±0.5	81.8±0.1	13.3±0.3	78.5±0.6	85.9±0.4	18.6±0.5
✓  I&T SFID	[66.6]±0.2	76.3±0.3	12.7±0.4	74.9±0.6	79.6±0.2	15.2±0.3
✓  I&T PromptArray	66.5±0.5	[76.5]±0.4	12.2±0.1	74.9±0.3	[81.6]±0.3	15.4±0.5
✓  I&T FairerCLIP	65.8±0.6	74.8±0.3	11.8±0.5	75.2±0.2	[81.6]±0.4	16.0±0.3
✓  I&T CLIP-clip	65.6±0.1	74.9±0.5	<b>[10.0]</b> ±0.6	[75.3]±0.3	80.8±0.4	<b>[13.2]</b> ±0.5
✗  T Orth-Proj	64.2±0.2	72.5±0.6	11.2±0.4	74.9±0.5	78.7±0.2	14.1±0.6
✗  T Orth-Cali	64.7±0.4	74.6±0.3	11.0±0.5	74.9±0.2	80.4±0.6	16.1±0.3
✗  I&T Ours	<b>[68.3]</b> ±0.5	<b>[78.4]</b> ±0.2	[10.1]±0.6	<b>[76.6]</b> ±0.4	<b>[85.1]</b> ±0.3	[13.6]±0.1

Table 8. Experimental results of BLIP on the zero-shot image classification task.

Datasets	CelebA			FACET		
Evaluation Metric	F1 $\uparrow$	$\Delta_{EO}^{Avg}$ (G×A) $\downarrow$	$\Delta_{EO}^{Max}$ (G×A) $\downarrow$	Macro F1 $\uparrow$	$\Delta_{EO}^{Avg}$ (G) $\downarrow$	$\Delta_{EO}^{Max}$ (G) $\downarrow$
Baseline BLIP	46.9±0.6	14.7±0.4	29.2±0.6	68.4±0.3	8.8±0.5	48.0±0.4
✓  I&T SFID	[52.5]±0.2	<b>[12.1]</b> ±0.1	26.4±0.3	60.6±0.1	8.2±0.2	47.1±0.5
✓  I&T FairerCLIP	52.1±0.4	13.4±0.6	<b>[22.6]</b> ±0.4	[61.0]±0.3	8.9±0.6	46.5±0.3
✗  I&T PRISM	[5]±0.5	13.8±0.2	26.1±0.5	60.3±0.4	<b>[6.8]</b> ±0.3	46.0±0.5
✗  I&T PRISM-mini	49.5±0.4	14.0±0.5	25.1±0.1	60.0±0.2	7.4±0.1	46.1±0.4
✗  I&T RoboShot	52.1±0.1	14.7±0.1	25.1±0.3	60.3±0.5	7.6±0.6	<b>[44.4]</b> ±0.1
✗  T Orth-Proj	48.2±0.3	14.6±0.2	27.0±0.2	58.3±0.2	8.5±0.2	46.3±0.2
✗  T Orth-Cali	49.6±0.6	14.4±0.1	27.5±0.6	59.5±0.3	8.0±0.6	46.0±0.5
✗  I&T Ours	<b>[54.8]</b> ±0.4	[12.2]±0.5	[23.2]±0.3	<b>[68.4]</b> ±0.3	[7.3]±0.4	[44.7]±0.3

Table 9. Experimental results of BLIP on the text-to-image retrieval task.

Datasets	COCO2017			Flickr30K		
	R@5 $\uparrow$	R@10 $\uparrow$	MS@1000 (G $\times$ ST) $\downarrow$	R@5 $\uparrow$	R@10 $\uparrow$	MS@1000 (G) $\downarrow$
Baseline BLIP	93.9 $\pm$ 0.5	97.2 $\pm$ 0.1	15.1 $\pm$ 0.6	93.9 $\pm$ 0.4	96.8 $\pm$ 0.2	18.3 $\pm$ 0.6
✓  I&T SFID	[90.6] $\pm$ 0.3	95.9 $\pm$ 0.4	12.5 $\pm$ 0.1	86.1 $\pm$ 0.6	89.9 $\pm$ 0.5	13.5 $\pm$ 0.1
✓  I&T PromptArray	90.4 $\pm$ 0.2	[96.0] $\pm$ 0.3	12.9 $\pm$ 0.4	86.4 $\pm$ 0.3	91.5 $\pm$ 0.4	12.8 $\pm$ 0.5
✓  I&T FairerCLIP	90.0 $\pm$ 0.6	94.7 $\pm$ 0.2	13.3 $\pm$ 0.3	[91.0] $\pm$ 0.2	[91.7] $\pm$ 0.3	12.0 $\pm$ 0.4
✓  I&T CLIP-clip	90.3 $\pm$ 0.4	94.5 $\pm$ 0.6	[11.2] $\pm$ 0.5	[91.0] $\pm$ 0.1	90.8 $\pm$ 0.1	[8.1] $\pm$ 0.2
✗  T Orth-Proj	90.8 $\pm$ 0.5	92.8 $\pm$ 0.4	13.5 $\pm$ 0.2	90.7 $\pm$ 0.6	88.1 $\pm$ 0.6	8.8 $\pm$ 0.3
✗  T Orth-Cali	90.3 $\pm$ 0.1	94.1 $\pm$ 0.5	13.7 $\pm$ 0.5	90.7 $\pm$ 0.3	89.9 $\pm$ 0.3	9.0 $\pm$ 0.1
✗  I&T Ours	[92.2] $\pm$ 0.4	[96.7] $\pm$ 0.2	[12.0] $\pm$ 0.3	[93.3] $\pm$ 0.5	[96.5] $\pm$ 0.6	[8.4] $\pm$ 0.5

## G. More Illustrative Examples

“A photo of a designer”



“A photo of a female designer”



Figure 9. Illustrative examples for  $o = \text{“designer”}$ . We randomly sample ten generated images for each method. Male-looking samples are marked in red and numbered. On the left, a more balanced ratio of female- and male-looking samples indicates lower bias, while on the right, fewer male-looking samples reflect better preservation of self-utility.

“A photo of a computer programmer”



“A photo of a male computer programmer”



Figure 10. Illustrative examples for  $o = \text{“computer programmer”}$ . We randomly sample ten generated images for each method. Female-looking samples are marked in red and numbered. On the left, a more balanced ratio of female- and male-looking samples indicates lower bias, while on the right, fewer female-looking samples reflect better preservation of self-utility.



Figure 11. Illustrative examples for  $o = \text{“civil engineer”}$ . We randomly sample ten generated images for each method. Female-looking samples are marked in red and numbered. On the left, a more balanced ratio of female- and male-looking samples indicates lower bias, while on the right, fewer female-looking samples reflect better preservation of self-utility.

“A photo of a CEO”



“A photo of a male CEO”



Figure 12. Illustrative examples for  $o = \text{“CEO”}$ . We randomly sample ten generated images for each method. Female-looking samples are marked in red and numbered. On the left, a more balanced ratio of female- and male-looking samples indicates lower bias, while on the right, fewer female-looking samples reflect better preservation of self-utility.